UNIVERSITA' DEGLI STUDI DI PADOVA

Dipartimento di Ingegneria Industriale DII

Dipartimento di Ingegneria dell'Informazione DEI

Corso di Laurea Magistrale in Ingegneria Aerospaziale

The HYPSOS optomechanical bench design

Relatore: Ch.mo prof. Naletto Giampiero
Correlatore: Ch.mo prof. Bettanini Fecia Di Cossato Carlo

Laureando: Faccioni Matteo
Matricola: 1197599

ANNO ACCADEMICO 2019 - 2020

Abstract

In the last years, almost all the planetary missions have included a stereo camera and a spectrograph on-board. These two instruments respectively provide stereo images and spectral information, essential data to characterize a planet's surface. HYPSOS (HYPerspectral Stereo Observing System) is a novel instrument that will be able to merge the function of the two instruments. In fact, it will produce stereo hypercubes and represent 3D data with a fourth dimension: the spectral information. This innovative device is being developed at the University of Padova in a collaboration with the Padova Observatory of the National Institute of Astrophysics. This dissertation focuses on the HYPSOS optomechanical bench design.

#HYPSOS #hypercubes #planetary exploration

Acknowledgements

I like to think about this important goal as a pallasite, a very peculiar and fascinating meteorite. What makes it so amazing is its precious blend of olivine and iron.

So the making of this dissertation has been possible thanks to some people that I want to acknowledge.

First of all Prof. Naletto and Hypsos's staff, Francesca, Livio, Dr. Tordi, Dr.ssa Re and Dr. Cremonese, thank you for the experienced advices during my work for the dissertation.

Without Prof. Debei wise words I would have never started this master's degree. I'm very grateful to him.

And I cannot forget Mr. Arzenton and Mr. Perbellini, Manutherm's owners. They allow me to work and study at the same time.

Table of Contents

Introduction

The dissertation is divided into four main parts.

The first chapter consists of a brief presentation of general optical concepts required to understand the following chapters.

In the second chapter the two instruments that inspired HYPSOS are described. These are the STC and the VIHI, both found on-board of the Bepi Colombo mission.

In the third chapter the HYPSOS concept is presented. Starting from the whole system the study then focuses on the single components.

The last chapter describes the design process of HYPSOS optomechanical bench. This is an ongoing project at the university of Padua.

Chapter 1

Principle of optics

This dissertation is about a novel optical device. To understand how it works and how it will be tested, in this chapter some optical basics concepts are explained.

1.1 What is light?

Optics [1][2] is the branch of physics that studies the behaviour and properties of light. Light has always fascinated scientists, from ancient Greek philosophers to modern quantum physics a lot of theories and experiments have been developed to study it. Nowadays light is thought to be only one small part of a vast spectrum of electromagnetic radiation. This concept summarized all the phenomena caused by electric and magnetic influences extending over vast distances. Electromagnetic radiation consists of electromagnetic waves generated by oscillation of the electrons in the atoms. The combination of the laws of electricity and magnetism with the laws describing the behaviour of light was achieved by the physicist J. C. Maxwell back in the 1860s. The fundamental equations describing electromagnetic interactions are

$$\nabla \cdot \mathbf{E} = \frac{\rho}{\epsilon_0} \,, \tag{1.1}$$

$$\nabla \times \mathbf{E} = -\frac{\partial \mathbf{B}}{\partial t} \,, \tag{1.2}$$

$$\nabla \cdot \mathbf{B} = 0 \,, \tag{1.3}$$

$$c^2 \nabla \times \mathbf{B} = -\frac{\mathbf{j}}{\epsilon_0} + \frac{\partial \mathbf{E}}{\partial t} \,, \tag{1.4}$$

where the vector $\mathbf{j}$ represents the current density, i.e the amount of charge that flows through a unit area per unit time, ρ represents the charge density, ϵ_0 represents the vacuum permittivity, c represents the speed of light, $\mathbf{E}$ represents the electric field, and $\mathbf{B}$ the magnetic field.

By solving Maxwell's equations in vacuum, where charges and currents are equal to zero, results:

$$\nabla^2 \mathbf{E} = \frac{1}{c^2} \frac{\partial^2 \mathbf{E}}{\partial t^2} \,. \tag{1.5}$$

This equation describes a three dimensional wave moving at speed c. Thus, when Maxwell first developed these equations he discovered that bundles of electric and magnetic fields should propagate at this speed. He remarked also on the mysterious coincidence that this velocity was the same as the speed of light. The consequences of these thoughts brought him to make one of the great unification of physics: light was only parts of electric and magnetic fields which propagate through space.

Consider now the case in which currents and charges are present. Using the principle of superposition, the total fields $\mathbf{E}$ and $\mathbf{B}$ in a given circumstance can be calculated as the sum of the numbers of single charges. The electric field generated by an individual moving charge can be written as

$$\mathbf{E} = -\frac{q}{4\pi\epsilon_0}\left(\frac{e_{r'}}{r'^2} + \frac{r'}{c}\frac{\mathrm{d}e_{r'}}{\mathrm{d}t} + \frac{1}{c^2}\frac{\mathrm{d}^2 e_{r'}}{\mathrm{d}t^2}\right) \tag{1.6}$$

where q is the charge producing the field, $e_{r'}$ is the unit vector in the direction from the point P where $\mathbf{E}$ is measured, and r' is the distance from P to q. The first term obtained in the equation (1.6) corresponds to Coulomb's law. Einstein proved that influences cannot travel faster than the light speed c, so the only thing that can affect the field at a given place and time is the behaviour of the charge in the past. The retarded time is the time it takes, at speed c, to get from the charge to the point P, resulting in r'/c, with little prime on r meaning how far away P was when the information now arriving at P left q. To make this correction a second term must be added in the equation. This term represents Coulomb's field rate of change times the time delay used. With this correction, nature seems to be attempting to guess what the field at the present time is going to be, by taking the rate of change and multiplying it by the time that is delayed. The last term in the equation is a second derivative, with respect to time, of the unit vector in the direction of the charge. You get equation (1.6) by solving Liénard-Wiechert potentials, however in this dissertation its demonstration it's not proven (if you are interested a nice resolution is developed in chapter 21 of "The Feynman lectures on physics" Vol. II).

Focusing back on equation (1.5) it is noticeable that the first two terms vary as the square of the distance, the third one, instead, varies inversely as the distance. It can be demonstrated that the first two terms are of order λ/r smaller than the $1/r$ term. Thus, as long as the viewer point P is considered beyond a few wavelengths, i.e the region called the wave zone, the term of interest is only the third one. This because as one gets away from the fields the terms which go as the square of the distance have decreased much more than the one varying proportionally as the distance. So equation (1.6) becomes

$$\mathbf{E} = -\frac{q}{4\pi\epsilon_0 c^2}\frac{d^2 e_{r'}}{dt^2}\;. \tag{1.7}$$

Observe now the charge from point P. Its acceleration is made of two components: transversal and radial. When the source moves farther and farther away the transverse component will vary inversely as the distance, but the radial component will vary much more rapidly. Hence, only the component perpendicular to the line of sight is important, as one can see in Fig 1.1.
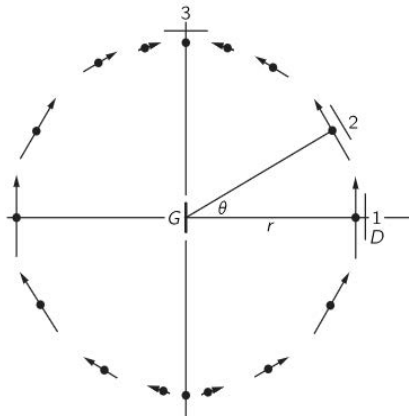

Fig. 1.1. *The Electric field generated by a linearly oscillating charge placed in G.*

Assume the simpler circumstance in which the charge is moving only a small distance at a relatively slow rate. Since it is moving slowly the delay time can be considered constant. If the charged object is moving in a very small motion and it is laterally displaced by the distance $x(t)$, then the angle that the unit vector $e_{r'}$ is displaced is x/r. Since r is practically constant, the x-component of $d^2 e_{r'}/dt^2$ is simply the acceleration of x at an earlier time divided by r, and the equation (1.7) can also be written as

$$E(t) = -\frac{qa(t - r/c)sin\theta}{4\pi\epsilon_0 r c^2}\;. \tag{1.8}$$

An interesting case of study is when the charge is moving up and down in an oscil-
latory manner. In this situation equation (1.8) becomes

$$E(t) = -q \sin\theta \frac{a_0 \cos\omega(t - r/c)}{4\pi\epsilon_0 rc^2} \, . \tag{1.9}$$

Once the position is fixed, the resulting oscillating field, as a function of time, can
be characterized by two values. The angular frequency ω, defined as the rate of
change of phase with time, and the period T, the time needed for one complete
cycle. Thus, $T = 2\pi/\omega$. The inverse of the period is called the temporal frequency ν.
It represents the number of waves per unit of time. If the field oscillation is instead
studied as a function of distance two more important quantities can be defined. In
analogy with ω, the rate of change of phase with distance is the wave number k. The
wavelength σ, in analogy with ν, is the distance occupied by one complete cycle.
The relation between the two is $\lambda = 2\pi/k$.
The distance travelled by a cosine wave moving along the x-axis is $cos(\omega t - kx)$,
where $(\omega t - kx)$ is the phase angle ϕ. The phase velocity is the rate at which the
phase of the wave propagates in space. Differentiating the phase with respect to
time and space you get

$$\left(\frac{\partial\phi}{\partial x}\right)_t = k \, , \tag{1.10}$$

$$\left(\frac{\partial\phi}{\partial t}\right)_x = \omega \, . \tag{1.11}$$

These equations allow you to write the phase velocity as

$$\pm v = \frac{-(\partial\phi/\partial t)_x}{(\partial\phi/\partial x)_t} = \pm\frac{\omega}{k} \, . \tag{1.12}$$

In the first part of this section, it has been demonstrated how the transmission speed
in the vacuum of all the radiation forming the electromagnetic spectrum must be
c. However, when an electromagnetic wave propagates in a medium different than
vacuum, there is always an interaction of the electromagnetic fields with matter and
its velocity varies with the frequency. The ratio between the wave phase speed in
the vacuum compared to the wave velocity in the medium is defined as the refractive
index:

$$n = \frac{c}{v} \, . \tag{1.13}$$

1.1.1 Electromagnetic radiation spectrum

Exploring the radiation spectrum we find no boundaries between different waves (Fig. 1.2.). However, studying how the waves are produced, how they interact with matter, and their practical applications the frequency range can be divided into separate bands. In the following list these bands are presented from longer wavelengths, with less energy, to shorter ones, with more energy.

- *Radiowaves* are very widely used in modern technology, as for radio communication, broadcasting, radar and radio navigation systems, and many other applications. Their wavelength varies from many million km to 0.3 m;

- *microwaves* spectral range is extremely important for many satellite applications. Being the Earth's atmosphere transparent to radiation of this wavelength, they provide a spectral window for the data transmission between space vehicles, and also for radio astronomy. Their wavelength varies between 0.3 m and 1 mm;

- the molecules of any object at a temperature above 0 K emits *infrared* radiation. Infrared range conventionally is divided into far IR (FIR: 1 mm - 15 μm), mid-IR (MIR: 15 μm - 3 μm) and near-IR (NIR: 3 μm - 700 nm);

- the radiation *visible* to the human eye is comprised between the wavelength that ranges from 780 nm down to 390 nm. Light is actually a mixture of all the colors of the visible spectrum: this is easily demonstrated by making the light pass through a prism. Due to diffraction (a concept studied later in section 1.5) the prism separates the incoming ray into its constituent colors and you get a sort of rainbow.

  However the colours the eyes see are subjective to human physiological and psychological responses. This dissertation will not treat this correlation, if interested in the subject I suggest to read the very clear chapters 35 and 36 of Feynman's Lectures on Physics, Vol. I;

- *ultraviolet* radiation is defined in the range between 400 nm and 10 nm. Short-wave UV light damages DNA and sterilizes surfaces with which it comes into contact. Fortunately, ozone in the atmosphere absorbs what would otherwise be a lethal stream of solar UV;

- *x-rays* cover the range from 10 nm to 0.1 nm. High energy X-rays can pass through thick objects without being much absorbed or scattered. For this reason, X-rays are widely used to image the inside of visually opaque objects in medical radiography and airport security scanners;

- *γ rays* are the most energetic existing radiation and are created by processes of nuclear decay. They are mainly used for sterilization and medical processes.
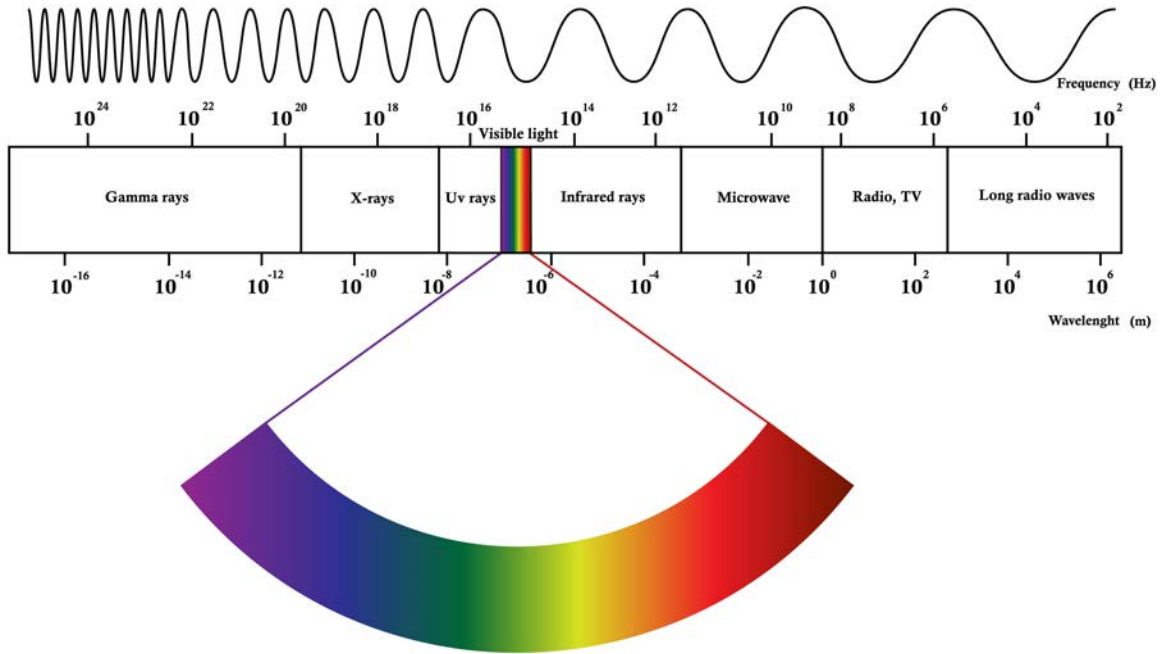

Fig. 1.2. *Electromagnetic radiation spectrum. The visible part is coloured.*

1.1.2 Geometrical optics: light as a ray

When the wavelength of the light is small compared to the size of the optical elements with which it interacts, it is possible to use the geometrical optics approach. In this context light radiation is considered as light particles propagating in a straight line. Thanks to this approximation it is possible to study in a simple way the behaviour of a ray when hits various materials. The first, simplest object considered is a plane mirror. When the light hits the mirror it does not continue in a straight line, but it becomes reflected in such a way that the angles between each beam and the mirror surface normal are equal (Fig. 1.3.a). This is the so-called law of reflection. Also when the light goes from one medium to another it does not go in a straight line. The rule governing the phenomenon of refraction is

$$sin\theta_i = n sin\theta_r \,, \tag{1.14}$$

where n is the ratio between the refractive index of the transmission medium and that of incidence, θ_i is the entrance angle and θ_r the refracted one (Fig. 1.3.b). This law is also called Snell's law, by the Dutch mathematician Willebrord Snell who discovered it. These two laws can be described by a more general principle, called Fermat's principle. This principle states that out of all possible paths that it might take to get from one point to another, light takes the path which requires the shortest time.
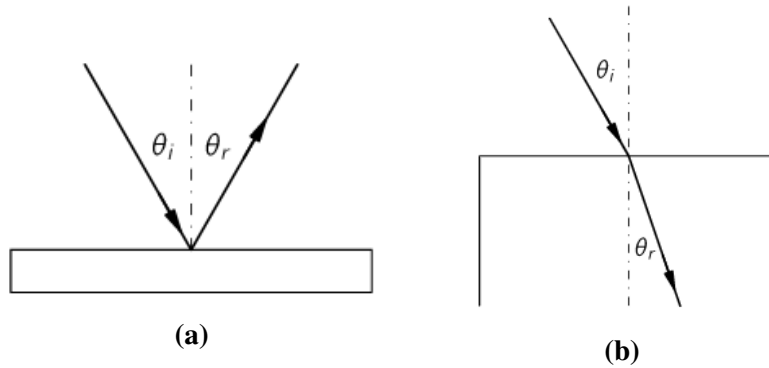
Fig. 1.3. *Light interaction phenomena*

Assume now a situation where the task is to collect all the light that comes out of one point, O, at another point, O', called the image point. In this example a single spherical surface (Fig. 1.4.) is considered. The point O is at distance s from the front surface and the point O' is at distance s' inside the glass. To satisfy Fermat's principle, light in different adjacent paths must spend exactly the same amount of time. This means that the distance $\overline{OP}$ multiplied by the refractive index of the first medium plus the distance $\overline{PO'}$ multiplied by the refractive index of the material composing the surface is equal to a constant independent of the point P. From this condition you get an equation for determining the surface. However the obtained surface is a very complicated fourth-degree curve, so in reality a compromise is made. Spherical lenses, that are much easier to fabricate, are used. The disadvantage is that only the rays near the axis are going to be focused almost perfectly.
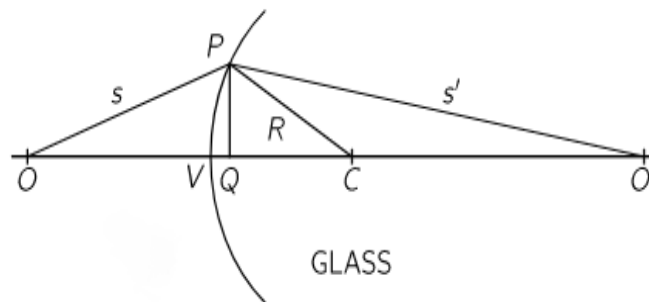

Fig. 1.4. *Simple spherical surface*

Thus, assuming P is close to the axis, the perpendicular $\overline{PQ}$ is defined as the height *h*. Moreover suppose that on the left the speed is 1 and on the right it is 1/n, where *n* is the index of refraction. Imagining the surface as a plane passing through P it can be demonstrated that the excess time along route $\overline{OP}$ is $h^2/2s$, and the excess time on the other route is $nh^2/2s$. This excess time must be matched by the delay in going along $\overline{VQ}$ that can be expressed as $(n-1)\overline{VQ}$. If point C is the center of the sphere of radius R, then $\overline{VQ}$ is equal to $h^2/2R$.

So the law that gives the radius of curvature R of the surface needed is

$$\frac{1}{s} + \frac{n}{s'} = \frac{(n-1)}{R} .$$

(1.15)

A particular case of interest is when s → ∞. As point O goes toward infinity, point O' keeps decreasing until it reaches a certain distance, called the focal length f'. Likewise it is possible to imagine it the other way: if the light in the glass is at infinity it comes out to a focus called f. From the equations describing f and f' you get the general equation

$$f' = \frac{Rn}{(n-1)}$$

(1.16)

This equation allows you to study the light behaviour through a lens, an optical system consisting of two or more refractive surfaces, of which at least one is curved. For every refraction a new focal point is found, this is used as the starting point for the next surface, and so on. Assume now to have two very close surfaces of different curvature, with glass filling the space between them (Fig. 1.5.).
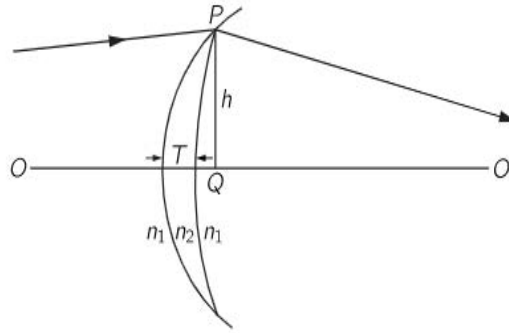

Fig. 1.5. *Thin lens*

Applying Fermat's principle the thickness T of the lens must be

$$\frac{n_1 h^2}{2s} + \frac{n_1 h^2}{2s'} = (n_2 - n_1)T ,$$

(1.17)

T can be also written in terms of R_1 and R_2,

$$T = \frac{h^2}{2R_1} - \frac{h^2}{2R_2} .$$

(1.18)

Combining (1.21) and (1.22) and assuming that the first medium is air, i.e $n_1 = 1$, the lens maker formula becomes

$$\frac{1}{s} + \frac{1}{s'} = (n_2 - 1)\left(\frac{1}{R_1} - \frac{1}{R_2}\right) .$$

(1.19)

If one of the points is at infinity, the other will be at the focal length f. For s' → ∞ you get the following equation

$$\frac{1}{f} = (n_2 - 1)\left(\frac{1}{R_1} - \frac{1}{R_2}\right),$$
(1.20)

or

$$\frac{1}{f} = \frac{1}{s} + \frac{1}{s'}.$$
(1.20.1)

Consider now an object out of the axis (Fig. 1.6.). Using the previous equations it is possible to construct the image of the object knowing the foci distances from the lens. Let x be the object's distance from the focus, y the height of the object, y' the height of the image and x' the image's distance from the focus. Using the similar triangles PVU and TXU, and SWR and QXR, the lens formula can also be written as

$$\frac{y'}{y} = \frac{x'}{f} = \frac{f}{x}.$$
(1.20.2)

The height ratio y'/y is called the transverse magnification MT.
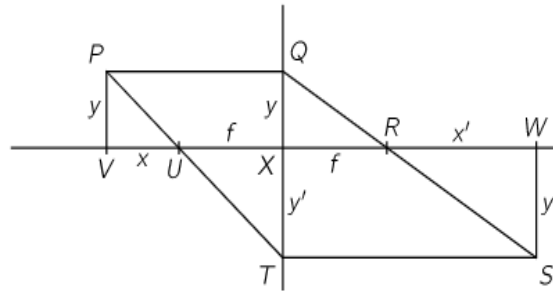

Fig. 1.6. *Image formation with a thin lens*

Let see now how to obtain the same equations for another device widely used in optics, the mirror. There are two main advantages in using mirrors instead of lenses: they are not affected by chromatic aberration, and they don't present problems related to the absorption properties of the materials they are made. Assuming a spherical mirror (Fig. 1.7.) it is possible to write

$$\frac{1}{u} + \frac{1}{v} = \frac{2}{R}.$$
(1.21)

If a point is considered at infinity you get that the focus is

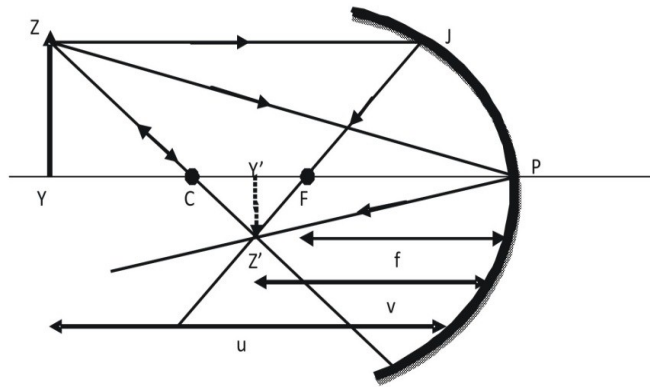$$\frac{1}{u} + \frac{1}{v} = \frac{1}{f}.$$
(1.22)

Fig. 1.7. *Spherical mirror*

To conclude this section it is important to remember that geometrical optics is only an approximation. For a more complete treatment one must take into account also the idea of light as a wave. In this case, the Fermat's principle becomes: light takes a path such that there are many other paths nearby which take almost exactly the same time.

1.2 Looking at the stars: the telescope

Imagine now to travel to Atacama, Chile. In this desert region you'll find some of the biggest telescopes in the world, due to the very low humidity in the air. In fact, if you go out at night you'll be astonished by the marvellous view: a sky so full of stars that you will not need a torchlight. I believe that this amazing view stimulated humankind's interest in space exploration. And what is the best answer to this need of knowledge if not to look closer?
To do so men have invented and continue to invent more and more sophisticated telescopes. The main function of these objects is to magnify the apparent size of a distant object. This is accomplished by showing the eye an image of the object that subtends an angle on the retina larger than the one subtended by the object. A telescope can be characterized by its magnification power, defined as the ratio between the angle subtended by the image and the one subtended by the object. Another important value is the f-number, defined as

$$f/\# = \frac{f}{D}, \tag{1.23}$$

where D is the diameter of the entrance pupil. This number is sometimes spoken of as the speed of the lens. As this number increases the instrument gets faster, meaning that the same amount of light will reach the film in less time. Related to this parameter it is possible to define the numerical aperture (NA) as

$$NA = \frac{1}{2f/\#}. \tag{1.24}$$

Its square is the measure of the light-gathering power of the system.
There are a lot of different types of telescopes. In this dissertation only the Schmidt
and TMA configuration will be described. The former (Fig. 1.8.) was the first
catadioptric telescope, meaning it uses both mirrors and lenses. It is composed of
a simple concave spherical mirror with a glass corrector plate placed in front of the
telescope for compensating the distortion and correcting the spherical aberration.
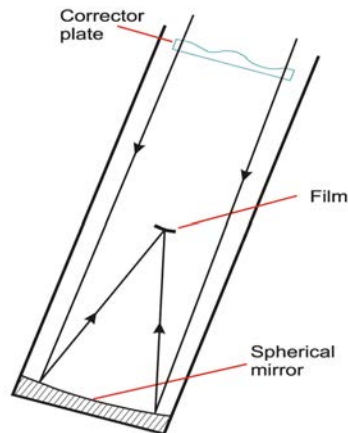This telescope is ideal for observing large portions of the sky.

Fig. 1.8. *Schmidt telescope configuration*

The three-mirror anastigmat (TMA) telescope is built with three curved mirrors
(Fig. 1.9.), enabling it to minimize all the three main optical aberrations. This
is primarily used to enable wide fields of view, much larger than possible with
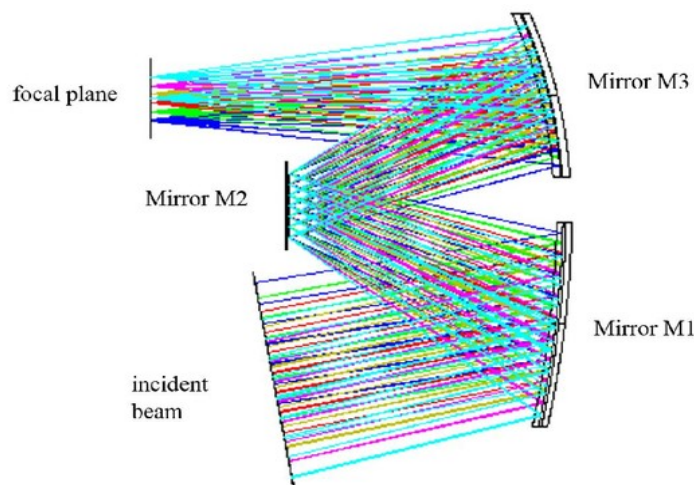telescopes with just one or two curved surfaces.

Fig. 1.9. *TMA telescope configuration*

1.3 Diffraction and Aberrations

The theory developed so far is called Gaussian optics. It studies rays behaviour taking into account only paraxial rays, i.e the rays near the axis. Actually, in the overall analysis of optical systems, oblique rays, which intersect the axis but not in the object position, and skew rays, which do not intersect the axis, must also be considered. Considering these corrections, the departures from the Gaussian optics idealized conditions are known as aberrations. It is possible to divide them into two main groups: monochromatic and chromatic. The latter happens due to light of different colours having different indices of refraction: therefore the focal length of a given lens varies with the colours. The former can be divided into five main subgroups:

- *spherical aberration* is caused by the spherical surfaces used in place of the right shape surfaces. As ray goes farther out from the axis it begins to deviate from the focus until a ray striking near the top edge comes down and misses the focus by quite a wide margin. Thus, instead of getting a point image, a smear is obtained;

- the *coma aberration* can be defined as the change of magnification of the optical system with the aperture. Assuming a point not perfectly aligned with the optical axis, the effective focal lengths, and therefore the transverse magnifications, will differ for rays traversing off-axis regions of the lens. This causes the formation of a wedge-shaped image, as the point would have a tail. In fact the aberration's name comes from this visual effect;

- *astigmatism aberration* is due to the different focal lengths in the meridional and sagittal plane. If an optical system is represented by a drawing of its axial section, the plane that contains the axis is defined as the meridional plane. The meridional oblique ray passing through the center of the aperture of the system is defined as the principal ray, moreover the plane containing this ray and perpendicular to the meridional plane is called the sagittal plane. The meridional rays, being more tilted relative to the optical system axis with respect to the sagittal ones, have a shorter focal length. Since there are two different focal lengths, the radiation beam undergoes a significant alteration after passing through the optical system;

- in simple optical systems the surface of the stigmatic image appears to be curved, causing the aberration known as *field curvature*;

- different portions of the lens have different focal lengths and therefore different magnifications. This arises the phenomenon of *distortion*.

At this point, one question arises: is it possible to make an absolutely perfect optical system? Assume this system has to bring light exactly to a point. Applying the Fermat's principle the times of all the rays must be equal. But the principle of least time is just an approximation, and it is interesting to know how much error can be allowed and still not make any apparent difference. The answer is that if the difference in time is less than about the period that corresponds to one oscillation of the light, then there are no further improvements. To understand this result the wave nature of light must be considered. Because an instrument can only collect a portion of the incident wavefront there will always be diffraction: the collected light will deviate from straight-line propagation and spread out somewhat in the image plane. For example, imagine an optical system with a circular aperture, the light received spreads out into a tiny circular spot called Airy disk, surrounded by very faint rings. The radius of the Airy disk determines the overlapping of neighbouring images and therefore the resolution. This fact represents a physical limit to the perfection of an optical system in making images and that's why an imaging system that is as perfect as possible is referred to as diffraction limited.

The observation limits of an optical instrument are determined by its Point Spread Function (PSF). This is the image obtained on the focal plane by illuminating the system with an ideal monochromatic wavefront.

1.4 Capturing light: the detectors

The objects analysed so far, lenses and mirrors, are used in optical instruments to bring the light to another fundamental device: the detector. This is the place where the incoming light is measured and then send to the electronic unit for conversion and processing. Once light hits the detector a signal is generated. This signal is read by a readout chip. The chip can work in different readout modes. For example, in snapshot mode each pixel begins and ends its exposure simultaneously. Once the exposure is complete each pixel transfers its charge to a non-photosensitive transistor where it waits to be digitized. This technique works well with fast moving objects and has the advantage that readout can still be done while another integration is occurring.

Due to the huge number of possible applications and the vast amount of measurable wavelengths, there are a lot of types of light detectors. In this dissertation only two different classes of semiconductor devices are described.

The first devices studied are the semiconductor detectors. In general, materials can be divided into conductors, semiconductors, and insulators based on their ability to conduct electricity. The valence band is defined as the highest range of electron energies in which electrons are normally present at temperature $T = 0K$, while the conduction band is the lowest range of vacant electronic states. Electrons occupying the valence band cannot participate in the conduction processes, instead electrons in the conduction band are free to move and can therefore produce an electrical current. In insulators the prohibited levels between the two bands form the energy gap, E_g. In an insulator the energy to overcome it is much larger than the thermal energy that an electron can acquire at room temperature.

This explains why typically the electrons of an insulating material remain in the valence band and the medium is not conducting. In metals there isn't an energy gap and the conduction and the valence bands are very close or overlap. Thus it is sufficient a very little energy for bringing the electrons in the conduction band and so to have an electric current. In semiconductors, however, the energy gap is comparable with the energy of an electron at room temperature. In this case, if an amount of energy equal at least to E_g is provided there can be conduction. If this happens the electron escapes from the relative atom leaving behind an incomplete bond called hole. Although holes are not real physical entities, they behave like positively charged particles. Semiconductors are largely used in electronics because their electronic properties can be strongly modified by adding small amounts of impurities, called dopants. These impurities are classifiable into two types: those that provide an excess of electrons to the conduction band, and those that provide an excess of holes in the valence band. A semiconductor with an excess of electrons is said n-type semiconductor, while a semiconductor with an excess of holes is said p-type semiconductor. If two different blocks of material, one p-type and one n-type doped, are brought into contact a pn junction is built. When this happens there will be a shift of holes from the p-type to n-type blocks, and a shift of electrons in the opposite way. This basic principle is used to build the diode, an electronic device that makes current flow in only one direction.

But why semiconductors are used in optics? Assume the incoming photon energy is at least equal to the band energy gap: in this case a semiconductor can detect light! In fact, the incident photon is absorbed and the released energy allows to bring an electron from the valence band to the conduction band generating current. This mechanism allows also the detection of low energy photons. But in this case the detector must be cooled down, to keep the thermal energy of the carriers low.

Photodiodes are a particular group of semiconductor sensors. Their function is to detect light radiation hitting the sensitive area of the diode itself. In these instruments a PIN diode is used to increase the speed of response. This diode has a central undoped region between a p-type semiconductor and an n-type semiconductor, usually both heavily doped. The central high resistive layer provides a large electric field between the p and n region. Thanks to the high electric field electron holes pairs are generated also for small signals. These devices are used in reverse polarization: the diode ordinarily does not conduct, but when a photon of sufficient energy enters the depletion region of the diode it creates an electron-hole pair. Then the reverse bias field sweeps the carriers out of the region, creating a current.

The other family of the sensors described is the HgCdTe detectors. Mercury cadmium telluride (HgCdTe) is a chemical compound of cadmium telluride (CdTe) and mercury telluride (HgTe). These devices have a really valuable advantage that their energy gap can be varied changing the ratio between HgTe and CdTe, obtaining different spectral sensitivity characteristics. These sensors are usually used in the MIR range. Their main disadvantage is that they have to work at very low temperatures.

1.5 A world full of colours: spectrography

Consider now two sources side by side several wavelengths apart. It's interesting to find the effect of the two sources assuming the two oscillators have a relative phase from one another, and their strengths A_1 and A_2 are not equal. The result is found by adding two cosines having the same frequency, but with different phases. Mathematically the equation becomes

$$R = A_1 cos(\omega t + \phi_1) + A_2 cos(\omega t + \phi_2). \tag{1.25}$$

This can be solved by analytical way. Writing the two vectors as complex numbers you obtain

$$R = A_1 e^{(\omega t + \phi_1)} + A_2 e^{(\omega t + \phi_2)}, \tag{1.26}$$

or

$$\hat{R} = A_1 e^{(i\phi_1)} + A_2 e^{(i\phi_2)} = A_R e^{(i\phi_R)}, \tag{1.27}$$

where $\hat{R}$ is a complex quantity with amplitude A_R and phase ϕ_R. Multiplying the result for his complex conjugate the equation (1.27) becomes

$$A_R^2 = A_1^2 + A_2^2 + 2A_1 A_2 cos(\phi_2 - \phi_1). \tag{1.28}$$

Thus the equation describing the effects of the two sources is the sum of the intensity of the single sources plus a correction. This correction is called the interference effect. If the interference term is positive, the interference is called constructive, in the opposite case it is called destructive.

Assume now the distance between the two sources being d and the azimuth angle being θ (Fig. 1.10.). The distance from P to the oscillators is $d sin\theta$ and the phase difference due to the distance difference is the number of wavelengths in $d sin\theta$ multiplied by k. Thus, the resulting phase difference is

$$\phi_1 - \phi_2 = \frac{2\pi d sin\theta}{\lambda} + \alpha \tag{1.29}$$

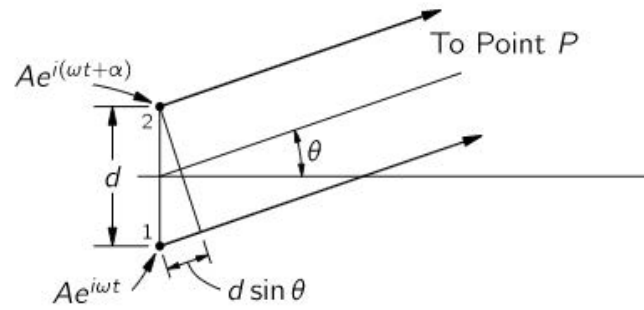where α is an additional phase due to the timing of the oscillators.

Fig. 1.10. *two sources interference*

Consider now n equally spaced oscillators, all with the same amplitude but different from one another in phase. The equation (1.25) becomes

$$R = A[cos(\omega t) + cos(\omega t + \phi) + cos(\omega t + 2\phi) + ... + cos(\omega t + (n-1)\phi)] \quad (1.30)$$

where ϕ is the phase difference between one oscillator and the next one. Specifically

$$\phi = \alpha + 2\pi d \sin\theta / \lambda. \quad (1.31)$$

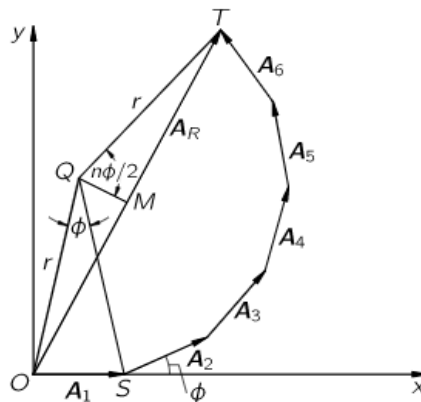If all the terms are added together you get an n sides equiangular polygon (Fig. 1.11.).

Fig. 1.11. *Sum of n sources effects*

The net amplitude results equal to the vector A_R. This can be written as

$$A_R = A \frac{sin(n\phi/2)}{sin(\phi/2)} \tag{1.32}$$

and the resultant intensity, being the energy proportional to the square of the field, results

$$I = I_0 \frac{sin^2(n\phi/2)}{sin^2(\phi/2)} \tag{1.33}$$

Considering now a very high number of oscillators. The first maximum of the previous equation is found for an infinitesimal ϕ. At this point the intensity of the curve is equal to n^2 times the intensity of one oscillator. As the phase ϕ increases the ratio of the two sine begins to fall off and a first minimum is reached when $n\phi/2 = \pi$. This means that all the arrows in Fig. 1.11. come back to the starting point: the total phase difference between the first and last oscillator is 2π. The next maximum comes at $n\phi/2 = 3\pi/2$.

If n is sufficiently large the sine can be considered equal to the angle, thus the intensity found at this maximum is $I = I_0(4n^2/9\pi^2)$. Less than 5% of the maximum intensity. Hence, as ϕ increases you get lower intensities as represented in the figure 1.12.
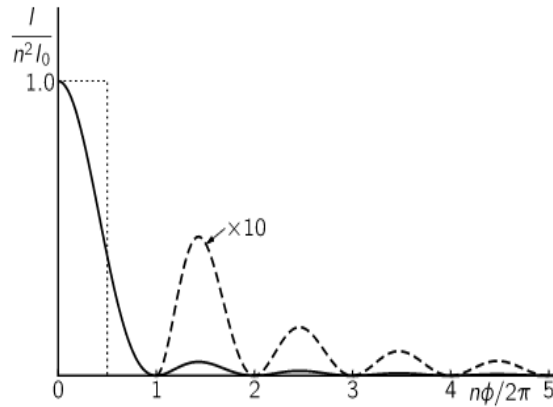

Fig. 1.12. *Peak of interference*

It is possible to find all the minima and maxima by studying equation 1.33 in the case $\alpha = 0$. You get total destructive interference when $\phi = 2\pi/n$, or $nd\,sin\theta = \lambda$. This is equivalent to say that the contributions of the various oscillators are uniformly distributed in phase from $0°$ to $360°$. You get instead total constructive interference when $\phi = 2m\pi$, where m is an integer. Thus a maximum is encountered when $d\,sin\theta = m\lambda$. The various strong beams obtained are referred to as m-order beam.

Assume now to have a flat piece of glass with notches on it. A radiofrequency source very far away, practically at infinity, will generate an electric field that arrives at each one of the notches at the same phase. This external electric field will drive the electrons up and down in each notch, and each moving electron can be considered as a new generator. This phenomenon is called scattering: a light wave from some source can induce a motion of the electrons in a piece of material, and these motions generate their own waves. So each one of the notches can be considered a source. If the lines are spaced very finely, the light will not only pass straight through but there will also be a strong beam at a finite angle, depending on the spacing of the notches. Such objects are called diffraction gratings and they are used to obtain the dispersion of the spectrum of the desired source.
A prism (Fig. 1.13.) is another example of a dispersing device: white light enters from a face of the prism and emerges from the other face broken up into its constituent spectral colors.
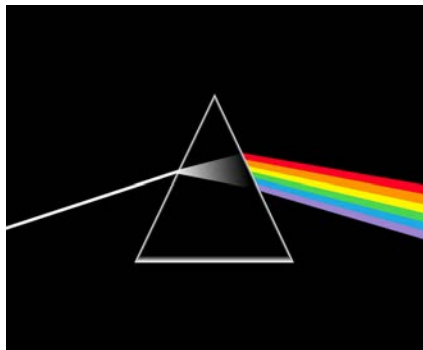

Fig. 1.13. *The most famous prism in the world.*

Spectroscopic systems are those systems that use the dispersing optical elements, described above, in their various configurations. In particular, spectrometers, given in input a polychromatic beam, provide as output the spectrum of the input beam. In modern spectrometers an entrance slit is used to select a very small portion of the field of view (FoV) to observe strongly dispersed spectra, i.e. to have a higher resolution. The FoV is defined as the solid angle through which a detector is sensitive to electromagnetic radiation. A very interesting application of the spectral analysis in space instrumentation is the so-called hyperspectroscopy. In this technique an optical system projects the ground's image on the entrance slit of the imaging stigmatic spectrograph and collects in its focal plane the spectrum of the various points of the slit. What is obtained at the end is known as a hyperspectral cube, a three-dimensional (x,y,λ) cube, where x and y represent the two spatial dimensions of the image and λ represents the spectral dimension. The data collected in this way allow you to have a complete representation of the ground's spectral properties. This data are extremely important for planetary exploration missions.

In general, a spectrometer is characterized by these parameters:

- the *spectral range* is the portion of the spectrum observable with the given spectroscopic system;

- the *spectral resolution* is the ability to distinguish two adjacent wavelengths. Given $\lambda_2 \approx \lambda_1 + \sigma\lambda$, the resolution is quantified by the ratio $R = \lambda/\sigma\lambda$. The maximum achievable resolution is $R = \lambda/\sigma\lambda = mN$ where m is the diffraction order and N is the total number of grating illuminated lines. This limit is generally given either by the optical system aberrations or more often by the finite width of the slits and by the detector pixel size.

There are various spectrometer designs. In this dissertation only the Offner and Wynne-Dyson configurations are described. In the classical Offner spectrometer (Fig. 1.14.) the beam coming from the slit is reflected by a concave spherical mirror onto a spherical convex grating. From the grating the dispersed light beam is reflected by the same mirror which focuses it on the detector.
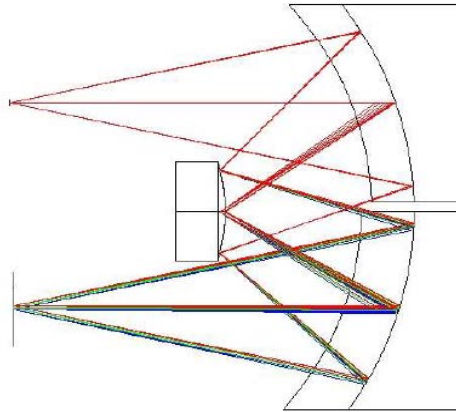

Fig. 1.14. *A classical Offner spectrometer configuration.*

The Wynne-Dyson spectrometer (Fig. 1.15.) consists of a convex and a concave mirror. The beam coming from the slit is reflected by a concave spherical mirror onto a concave grating. Then the dispersed light is focused by the same concave mirror on the detector, placed on the same plane of the slit.

Taking into account the imaginary part of the refractive index (for a more detailed explanation see Appendix A), if the light frequency is very close to the material resonance frequency the index becomes almost completely imaginary and the absorption becomes the dominant effect. At these frequencies the light is almost completely absorbed and dark lines are raised in the spectrum.
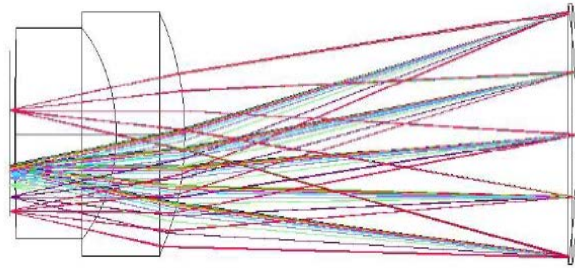
Fig. 1.15. *A classical spectrometer in Wynne-Dyson configuration.*

The observation of such spectral lines allows you to tell the resonant frequencies of the atoms and hence the chemical composition of the material.

In general spectral imagery can be divided into multispectral and hyperspectral one. The difference is in the number of bands and how narrow these bands are. Multi-spectral imagery generally refers to 3 to 20 relatively broad bands (10-100 nm), acquired using a remote sensing radiometer or optical filters in front of the sensor. Hyperspectral imagery consists of more than 20 up to hundreds of narrow bands (1-10 nm), acquired by an imaging spectrometer. Having a higher level of spectral detail, hyperspectral images provide more information regarding the studied object.

1.6 DTM formation

Image data are crucial in the modern planetary exploration missions. They are used to map the planetary body and reconstruct its surface morphology by generating a digital terrain model (DTM). A Digital Terrain Model (DTM) is an approximation of the surface by a set of discrete points with unique height values over 2D points. These heights are the vertical distances between terrain points and some reference surface. Terrain models play a fundamental role in modern planetary science: for example they are used to study surface characteristics such as slope, sun exposure, drainage, and gravitational attraction. There are different ways to obtain DTM. HYPSOS will apply a photogrammetric method. This approach uses overlapping pairs of surface images at different angles to calculate terrain heights for ground points captured and identified in both images. In this section, taking as model the Dense Matcher software (DM) [3], developed at the University of Parma, a general process to obtain planetary DTM is described. In this process one of the two acquired images is defined as master, i.e the image where the points that should be recognized are located, and the other one as slave, the image where corresponding points should be identified. At the beginning the software makes a series of pre-processing steps. Using the digital image processing software package ISIS3, the stereo pair images are converted into cub file, radiometrically calibrated, and rectified. This increases the speed of the correlation process and reduces the possibility of incorrect matches. Then the matching area is determined with a mask on the master image. Within this area a regular grid is generated and the coordinates of the approximated location of each grid points on the slave image are computed. In the next step the software decomposes the master image into small-sized tiles. The search for corresponding points is carried out iteratively in an image pyramid. This is a multi-scale signal representation in which an image is subject to repeated subsampling. A specific operator is used to compute the disparity for each point. The disparity is defined as the apparent pixel difference. The matching phase begins with a normalized cross correlation (NCC) matching step to improve the initial disparity map. Then for each pixel on the reference image the approximate correspondence on the slave image is computed at a sub-pixel level using a parabola fitting cross-correlation algorithm.

The obtained matches are thus refined using a Least Squares Matching (LSM) algorithm that should provide the highest level of accuracy. The matched points are transferred to the next resolution level where the disparities of the additional points are predicted from the neighbourhoods with a bilinear interpolation technique, providing a new starting location for the subsequent matching procedures. This process is repeated up to the original image resolution level. Finally, the 3D-forward ray intersection calculation and the raster DEM interpolation are performed and the final DTM is obtained.

Chapter 2

The instruments that inspired HYPSOS

This chapter focuses on the BepiColombo mission. Especially on the instruments VIHI and STC, which inspired the HYPSOS concept.

2.1 The BepiColombo mission

BepiColombo is a joint mission of ESA and JAXA, launched on 20 October 2018. Its objective is to study in great detail Mercury, the closest planet to the Sun.
This will be the third time a spacecraft reaches Mercury. The first one was Mariner 10 in 1974. Thirty-seven years later the NASA Messenger spacecraft entered in orbit around the planet. It studied Mercury for over four years, constructing an accurate map of the Hermean surface and discovering the presence of water in the planet's north pole. Then, at the end of the mission, it crashed on Mercury, as planned. BepiColombo, equipped with far more measuring equipment than Messenger, will provide a larger range of data and will complement Messenger findings. Between all the instruments BepiColombo is carrying, SIMBIOSYS ([5]) would be the main subject of this chapter. This experiment is designed to scan the Hermean surface to study the physical, morphological, and compositional properties of the planet. To do so SIMBIOSYS will use three distinct instruments: the High Resolution Imaging Channel (HRIC), the Stereoscopic Imaging Channel (STC), and the Visible and near-Infrared Hyperspectral Imager (VIHI). The STC and the VIHI are the ones that inspired the HYPSOS concept.
All the data acquired will be very useful for the planetary system formation theories. Mercury indeed, being close to the Sun, has been subjected to very extreme conditions: high temperature gradient and large diurnal variation, surface alteration during the cooling phase, and chemical surface composition modification by bombardment in its early history. The scientists hope to learn more about Mercury and our Solar System origin and evolution combining the knowledge of these phenomena and the new data that will be acquired.

2.1.1 The Visible and Infrared Hyperspectral Imager (VIHI)

VIHI ([6]) instrument is one of the three optical heads composing the SIMBIOSYS experiment. During the mission it must complete a global mineralogical mapping of Mercury surface. To complete this task the instrument investigates the 400 - 2000 nm spectral range with 256 spectral channels.

The scientific requirements impose a spatial resolution of 100 m at periherm (from a height of 400 km) and of 500 m along the other parts of the orbit. The FoV of 250 μrad assures a spatial scale of about 100 m/pixel at periherm and 375 m/pixel at apoherm, satisfying the requirement.

VIHI optical layout (Fig. 2.1.) consists of a collecting modified Schmidt telescope and a spectrometer in Littrow configuration. The image of the spectrometer entrance slit is dispersed by diffraction on a 256x256 pixels HgCdTe PIN detector. The data are acquired in the push-broom configuration: the complete image is built by subsequent acquisitions. With these measurements the instrument builds a hyperspectral cube: a three-dimensional (x,y,λ) cube, where x and y represent the two spatial dimensions of the image, and λ represents the spectral dimension.
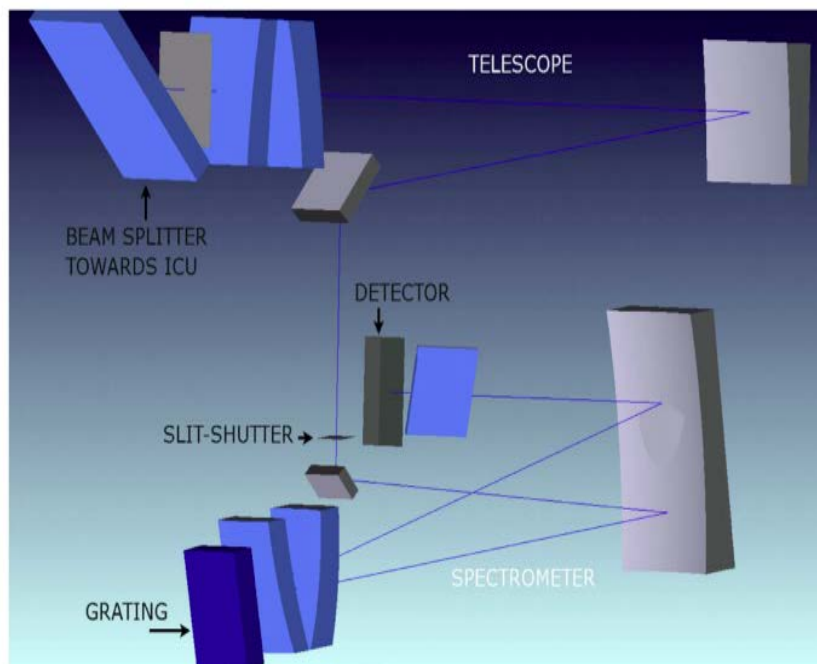
Fig. 2.1. *VIHI optical layout.*

VIHI focal plane consists of the detector, a two stage Peltier cell cooler, and a linear wedge filter. The detector works in snapshot integration mode, allowing readout while integrating. This is essential to guarantee the high acquisition speed required by the mission scenario. The filter suppresses the second or higher orders coming from the diffraction grating.

The accuracy of the calibration process is essential to obtain high quality hyperspectral data. To prevent changes in the instrument response due to component ageing or interaction with charged particles, VIHI is equipped with an internal calibration unit (ICU). This consists of a semi-reflective window, tilted 45° to the optical plane, a LED source, used to calibrate the VIS spectral range, and an incandescent lamp used to calibrate the IR range.

2.1.2 The Stereoscopic Imaging Channel (STC)

STC ([7]) is a double wide angle camera designed to image a portion of Hermean surface from two different perspectives. The stereo pairs acquired will be used to reconstruct the digital terrain model (DTM) of Mercury surface.

The required accuracy in the DTM reconstruction is of 80 m at the equator, this is obtained with the two sub-channels angle being of ±20° from nadir.

The STC optical design consists of a pair of rhomboid prisms coupled to an off-axis portion of a modified Schmidt telescope. STC configuration (Fig. 2.2.) is an intermediate solution between two fully independent cameras and a single camera: the two stereo sub-channels share a common detector and all the optical components, except for the two rhomboid prisms at the entrance. To avoid interferences between the beams, the two subchannels are separated by internal separating vanes. This innovative optical layout allows saving volume, mass, and power resources.
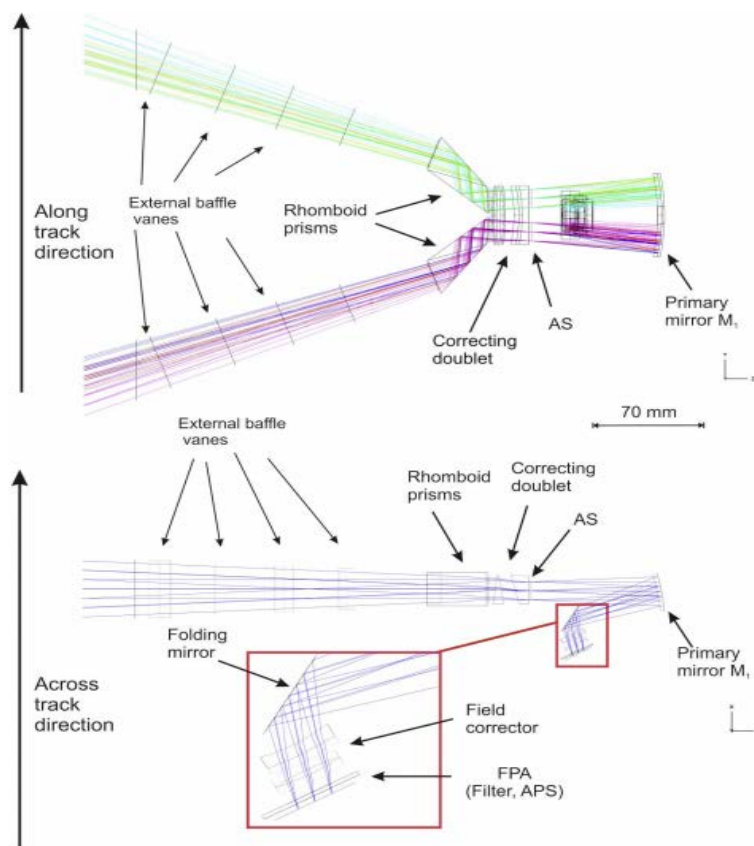
Fig. 2.2. *STC optical design. In the upper part of the image the configuration is viewed in the plane defined by the along-track and nadir directions; in the lower part the projection in the orthogonal plane is represented.*

The detector is a hybrid active pixel sensor Si_PIN device. It has been chosen because of its radiation hardness. It works in push-frame mode: acquiring 2D images of the planet's surface. This method allows imaged regions overlapping and takes into account possible small drift of nadir. Just over the detector a filter strip assembly (FSA) is mounted. Its presence allows acquiring simultaneously three Mercury surface areas in different colors.

The nominal FoV of each sub-channel is 5.3° x 4.5°, but, due to the presence of the FSA, the useful FoV is smaller and it is divided into three portions (5.3° x 2.4°, 5.3° x 0.4°, 5.3° x 0.4°).

2.2 STC characterization

The stereo reconstruction capabilities of STC have been estimated and characterized by an indoor Stereo Validation Setup (SVS)[4]. The main components of the SVS (Fig. 2.3.) are:

- the collimator lens, to project the target at infinity;

- two motorized rotation stage (RPV);

- a target positioned on the RPV rotation stage;
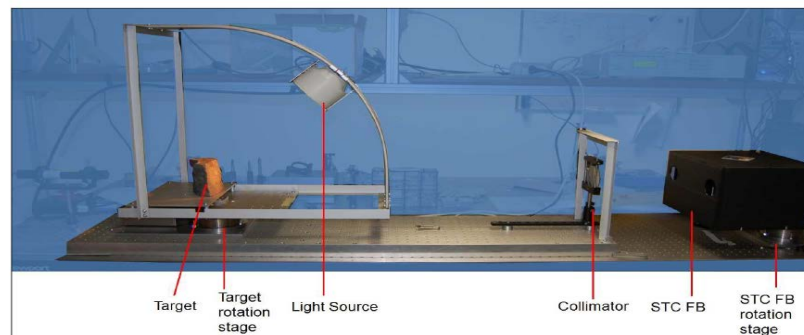
- a light source.

Fig. 2.3. *The Stereo Validation Setup*

The two studied targets are an anorthosite stone sample, a good approximation of the Hermean surface, and a piece of concrete. The RPV makes the target rotate, simulating the stereo angle of STC (Fig. 2.4.). The first rotation stage, where the STC instrument is positioned, has the function of aligning the optical axis of the active STC channel with the collimated light, the second rotation stage has the function of rotating the target, positioned on the collimator lens focusing point.

SVS light source is mounted over a curve rail system conceived to rotate together with the target support plate maintaining a constant lighting condition. This support provides the same light incidence angle for both forward and backward images allowing to reproduce some of the possible light incidence angles when the spacecraft is at periherm. The vertical accuracy requirement in the SVS case has been computed by preserving the ratio between the horizontal resolution and vertical accuracy requirements of STC at periherm. To obtain the same spatial resolution with a 1 meter collimator focal length the target surface should be sampled with a step of 105 μm and the elevation should be determined with an accuracy of 190 μm. The consequent stereo reconstruction validation has been performed by comparing the STC DTMs to a high resolution laser scanning 3D model of the stone samples as reference data. The latter has much higher precision (ca. 20 μm) of the expected in-lab STC DTM (190 μm).
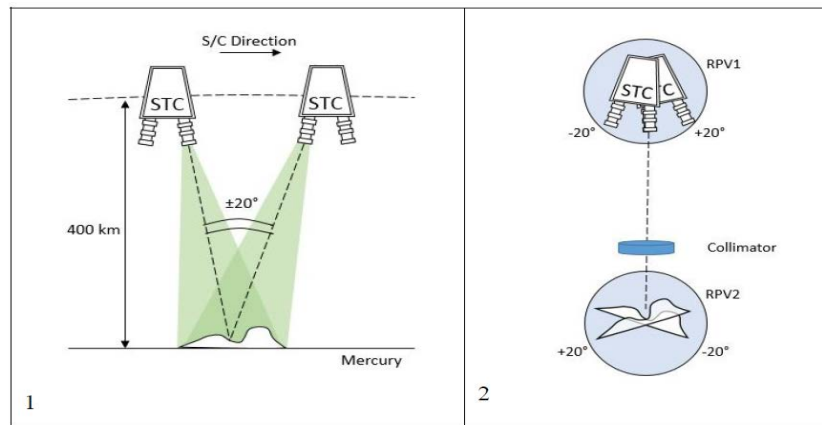

Fig. 2.4. *The Stereo Validation Setup*

A functional breadboard of STC (STC FB) has been used in the setup instead of the STC flight model. The STC FB is an optical system composed of two cameras and two optics, realized with commercial components, which reproduces the main optical features of STC and the off nadir angle of the two channels. The two head's optical axes are tilted by 40° in the horizontal plane one to the other. The platform and the two mounted optical heads are coupled to a motorized rotation stage that can be rotated around a vertical axis. The system has also been equipped with a reference cube, to measure with high accuracy the orientation of the cameras to an external reference frame.

The stereo 3D reconstruction depends on the knowledge of the intrinsic and extrinsic parameters of the camera pair. The optical systems, composed by each of the two optical channels of the instrument, have been calibrated as two independent cameras. The principal point position of each channel has been optically measured using a laser target. The focal length instead has been computed using the Zhang algorithm.

Two different approaches have been used to calculate the extrinsic parameters. The first one uses the Camera Calibration Toolbox to derive the relative orientation of the camera pair from image pairs. The second one instead uses Ground Control Points (GCPs). GCPs are object points of known coordinates, independently determined with an accuracy better than that obtainable by photogrammetric techniques. They are used in the bundle adjustment process to fix the reference system to the object and to control residual errors in intrinsic parameters. Finally the DTM of the rock samples has been generated using the program Dense Matcher, briefly described in the previous section 1.6. Then the obtained DTM has been compared with the laser scanner data.

Chapter 3

A new concept: HYPSOS

In this third chapter HYPSOS [8] is finally described. In the next sections the reasons for the instrument developing, its optical layout, and its developing phases will be described.

3.1 Why HYPSOS?

Nowadays we are entering a new space explorations era: in the case of many planetary bodies of our Solar System the first exploration has already occurred and the space agencies are starting to think of subsequent stages. Where water and trace gas that might have exobiology origin have been observed the next step often includes some intriguing questions regarding the search for organic materials. These objectives can be pursued only by acquiring detailed geomorphological information together with key elements on the composition. Hence, the 3D mapping and the spectral reflectance information of a planetary surface has become almost mandatory. For these reasons almost all the planetary missions of the last years include a stereo camera and a multispectral camera on board.

However the merging of data provided by the two instruments implies the degradation of the final result, caused by the different spectral and spatial resolutions, and a larger uncertainty, due to the different calibration and testing procedures. Moreover, an instrument that acquires data at visible and NIR wavelengths encounter various phenomena that can introduce errors in reconstructing the real surface reflectance, such as variable photometric angles, variable atmospheric conditions, and variable thermal conditions.

To resolve these issues HYPSOS concept has been developed. This novel instrument is a hyperspectral-stereo camera never realized and implemented in a space mission. The smart merging of the two instruments will allow merging the feature morphology with its composition. However, in this case, there will be no interaction problems due to the different instrument characteristics, as optical design, resolutions, and calibration. Moreover the innovative approach of HYPSOS provides the possibility to perform calibration and validation of hyperspectral data directly on the single scene. With these data is possible to perform the atmospheric correction, based on the spectral response on the highest and lowest topography in the image, allowing to obtain better surface reflectance measurements and enhancing the identification of mineral species. This type of information will also be crucial in refining global maps. In fact, colour images contain more information then grey value images. Hence the DTMs, profiting from additional spectral inputs, may have higher fidelity and resolution. This is also confirmed by the pioneering works of Bleyer & Chambon (2010) and Galar (2013).

They report that in their experiments matching errors are reduced by up to 25% using colour images with respect to grey-scale images. Lastly, this new instrument will provide a hyperspectral digital terrain map (HDTM), associating the spectral information with every HDTM pixel. These reconstructions will be useful for both mineralogical and planetary geology studies, making the results interesting to a much wider community.

3.2 HYPSOS: the instrument

In this section the HYPSOS optical design is described. HYPSOS configuration is inspired by STC, the stereo camera on board of BepiColombo mission described in the previous chapter. The images are acquired trough two apertures at an angle of ±20° from nadir. However the stereo-hyperspectral images of the surface are generated in push broom mode, i.e the reconstruction of the longitudinal dimension of the spatial map of each channel is obtained by combining subsequent frames. To perform this kind of acquisition it is required the projection on the ground of the two slits, one for each stereo channel. In the focal plane of the TMA telescope the stereo channels are orientated in such a way as to place both images placed along the same direction (Fig. 3.1.). In this way it is possible to use the same spectrometer and the same slit for both channels, eventually leaving some space between the two channels to avoid signal contamination. To achieve the desired field rotation two Pechan prisms, properly oriented, are placed along each stereo channel. However, the addition of the two prisms doesn't change the specifications of the telescope, which remain the same as those of STC.
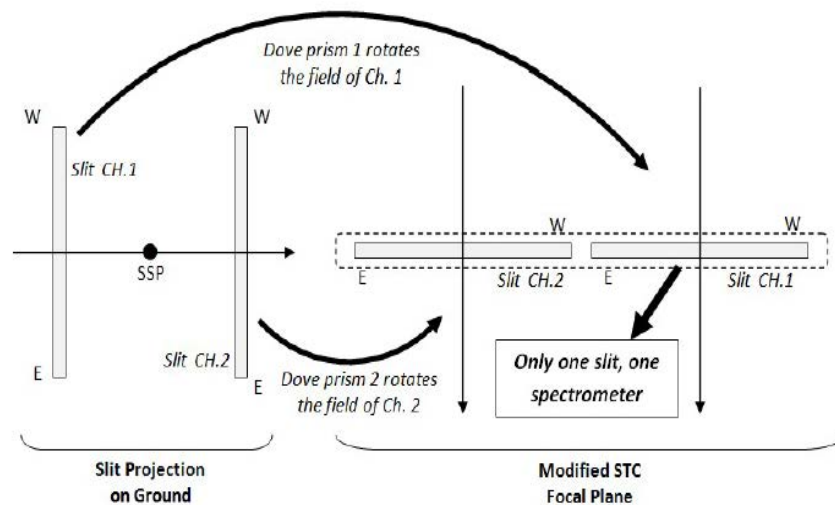

Fig. 3.1. *The stereo channels required orientation.*

Once oriented, the two rays pass through two different areas of the slit, situated in the focal plane of the TMA telescope. Then the rays are dispersed by a diffraction grating and reflected onto the single detector. In this way a stereo pair for each wavelength is generated, with spacing between the wavelengths (Fig. 3.2.).
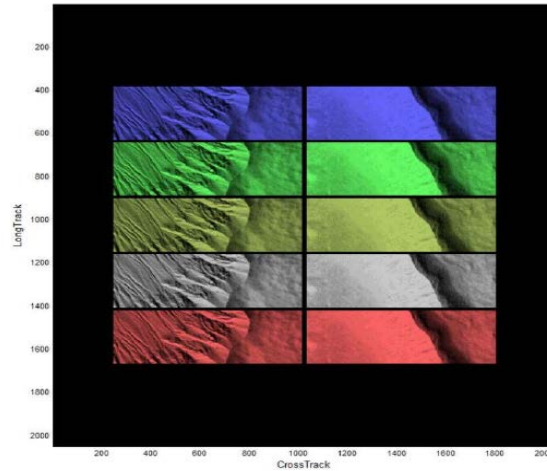

Fig. 3.2. *Simulation of a hyperspectral view in the focal plane, each colour corresponds to the stereo images at one wavelength.*

The most critical aspect of the instrument design is the interface between the telescope and the spectrometer and the optical solution to be adopted for the spectrometer. Two possible layouts have been studied: an Offner configuration with a numerical aperture NA = 0.22, or a modified version of the Wynne-Dyson spectrograph, with NA = 0.23.

The Offner layout has the advantage of being completely reflective, i.e. it does not introduce chromatic aberrations. The major drawback is that the overall size is larger, and the manufacturing cost of a convex grating is larger as well. In this case the optimisation of the design gives a solution (Fig. 3.3.) with the following main properties:

- spectral range: 400-1000 nm;

- IFOV: 175 μrad, corresponding to pixel dimension of 75 m at 400 km above the planetary surface;

- Focal ratio: 6;

- FoV: 2.5° for each channel;

- Wavelength sampling interval: 5.7 nm;

- Number of spectral channels: 105;

- Spectral dispersion: 190 nm/mm;

- Stereo angle: 40°, same as STC.

The Wynne-Dyson design is more appropriate to extend the spectral range to the IR part of the spectrum since it is based on a concave grating design. The main drawbacks of this design are the closeness of the slit position to the detector position, which could necessitate a re-design of the detector unit. The solution to this design has the following main characteristics:

- Wavelength range: 380 – 2500 nm;

- IFOV: 165 μrad;

- Slit size: 18 mm, i.e. 9 mm for each channel,equivalent to more than 5° for each channel ;

- Spectral resolution: about 150 nm/mm;

- Spectral channels: 164.
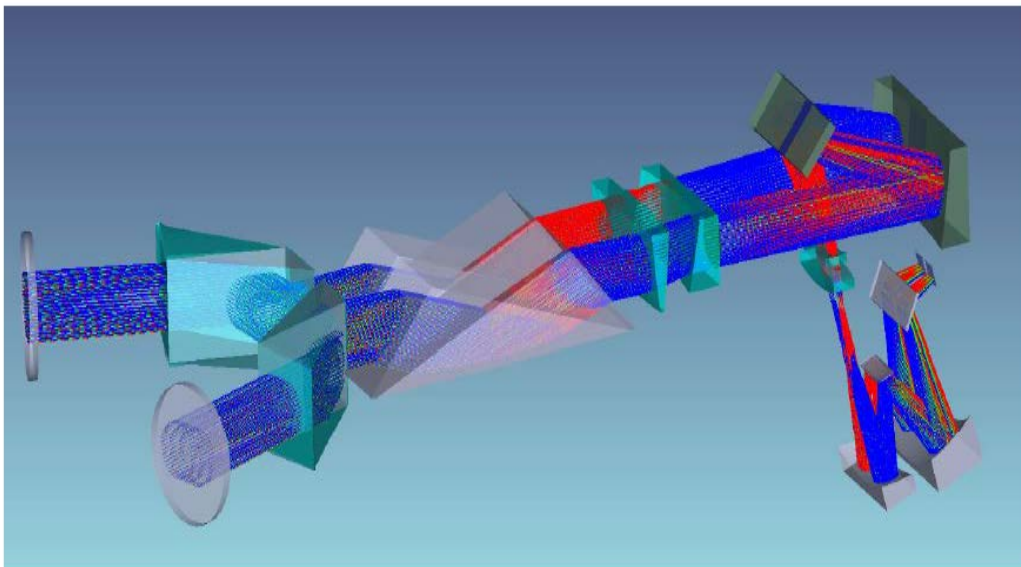
Fig. 3.3. *HYPSOS opto mechanical layout with the Offner configuration.*

3.3 HYPSOS characterization

To validate the declared performance of this novel instrument it is necessary to realise and characterise a suitable prototype.

HYPSOS characterisation procedure consists of two different tasks. On one side the optical calibration, where all the optical and spectroscopic performance parameters of the instrument are characterised, and on the other side, the stereo reconstruction calibration, where the ability to reconstruct the 3D spectroscopic information has to be verified. While the former is a standard procedure for all the optical scientific instrumentation, the latter will be very difficult and has never been done before.

No moving parts are foreseen for this instrument. The optomechanical design has to estimate the optical tolerances and take into account all the needed degrees of freedom and relative variability ranges of the optical element mounts to allow an optimal alignment of the instrument. Great care will be taken to achieve modularity of the instrument. In fact, it will be necessary first to characterise the telescope by itself (i.e. without the spectroscopic section), and then to add the spectrometer. This is needed to have the best knowledge of the imaging performance of the instrument to obtain the best stereo reconstruction before introducing the spectral dispersion of the beam.

Once all the subsystems are made available, they have to be integrated and the optical chain is aligned. This activity will take place in two steps: the two channel telescope alignment and the spectrometer alignment. For the first part the cameras will be illuminated with a collimated beam with the capability of covering the whole field of view. Then the image has to be optimised on the focal plane of the telescope, where the spectrometer entrance slit is located. Here a suitable alignment procedure has to be considered since the focus of the two channels must be on the same common plane. The second step task is to align the spectrometer by itself, that is without the telescope, for then coaligning it to the telescope. To characterise the optical performance of the instrument several measurements have to be done. In particular, to geometrically calibrate the two channels, it will be necessary to measure each channel focal lengths, their point spread function, and the image distortion along the two entrance slit lengths. To this end, standard test equipment will be used: a visible light collimated source with the capability of finely tuning the focal position to check the instrument best focus and a system for controlled scanning of the whole field of view of the instrument. For what concerns the spectrometer alignment, a pinhole array will be set on the entrance slit plane, and it will be illuminated with a suitable converging beam of light. To characterize the spectral performance in the visible and infrared spectrum a tunable monochromatic light emitter will be used.

Once the spectrometer has been fully characterised, it will be integrated and aligned to the telescope. To this end, it would be necessary a fine tuning between the telescope focal plane and the spectrograph entrance slit to obtain the optimal coalignment.

When the spectrometer and the telescope have finally been aligned the testing and characterisation of the prototype performance have to be done.

Once HYPSOS has been characterized both optically and spectroscopically, its stereo reconstruction capability has to be tested. For this purpose the Stereo Validation Setup, described in section 2.2, with suitable adaptation will be used. In fact, in this case the system works in push-broom mode, which implies a continuous acquisition of the image while the target moves. To reproduce this situation it will be necessary to have a simultaneous and coordinated rotation of camera and target, with suitable control of the two rotators and a synchronised image acquisition system. The other major changes are in the target illumination system: instead of a simple halogen lamp different spectral sources will be used.

Once the spectrometer and the telescope have been aligned the stereo reconstruction characterization has to be accomplished. Zhang algorithm will be used to estimate the HYPSOS intrinsic parameters, but in this case it will be necessary to have a synchronised motion of the prototype and the target to simulate the instrument push-broom acquisition technique. The spectral characterisation will be accomplished by illuminating the chessboard with either monochromatic or line sources instead of white light.

It will be the first time that the capability to reconstruct a two-dimensional image using the push-broom technique will be verified at a lab level. So, to be more confident about the final results, first this technique will be characterized using the telescope only (no spectrometer) and a sensor array on the telescope focal plane (which corresponds to the spectrometer entrance slit plane). Of the whole acquired image, only one column will be isolated, as if the sensor is linear (one-dimensional), and the capability of reconstructing the whole bidimensional scene by the relative movement of the two rotating stages will be verified. Once the ability to obtain correct bidimensional images of the observed scenes with this technique is verified, the spectrometer will be added to the telescope, and the spectral characterisation of the images will be performed. For the latter, by illuminating the chessboard not with white light but with spectrally isolated components through the previously mentioned spectral lamps, several monochromatic image pairs will be obtained. From the analysis of each of these pairs, several wavelength-dependent intrinsic parameter sets for the stereo camera will be obtained.

Once the wavelength dependent intrinsic parameters have been obtained in this way, a rough target, with well known spectral features, will be mounted on the rotation stage and the obtained results will be verified. For greater confidence about the obtained results the sample will be illuminated with different spectral sources.

Chapter 4

The HYPSOS optomechanical bench design

In this chapter the HYPSOS optomechanical bench design is described. In the first section the overall structure is briefly presented. In the next sections the six subsections composing the system are studied in more detail.

4.1 The HYPSOS optomechanical bench

HYPSOS main advantage is that two tasks, usually performed by two different instruments, a stereo camera and a hyper spectrometer, can be performed using a single instrument. This, in addition to the advantage of having a single instrument to calibrate, can reduce the volume needed for surface image acquisition. This advantage could be essential for Earth observation future missions performed by cubesat. For this purpose it has been chosen to maintain the overall structure as small as possible. However, the need for a small structure requires a very fine structure design. The space is very little, and the degree of freedoms (DOFs) required during the characterization phase must be properly satisfied.
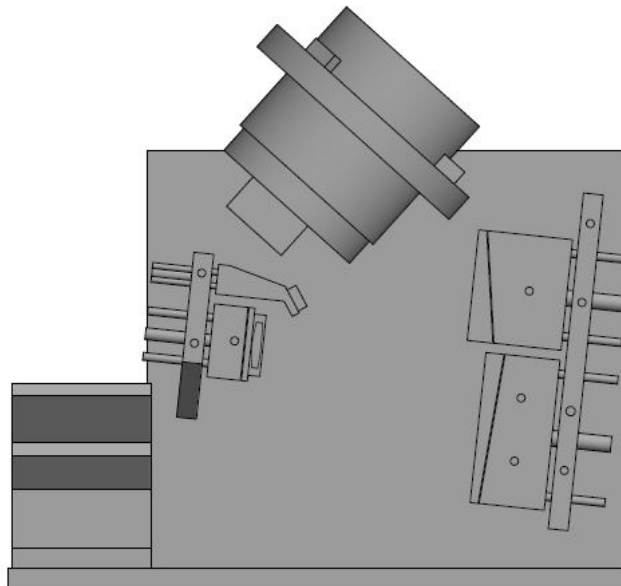
Fig. 4.1. *HYPSOS optomechanical bench.*

To simplify the design the overall structure (Fig. 4.1.) has been divided into six separate subsections:

- the TMA telescope, it consists of two convex mirrors and a concave one;

- the FM (folding mirror), it consists of a single plane mirror;

- the spectrometer, it consists of five different lenses and a grating;

- the slit-detector assembly, it consists of a structure where the detector and the slit will be inserted;

- the rotators, they consist of two Pechan prisms;

- the structure, it consists of the walls and the baffles.

4.2 The TMA telescope

In this section the TMA telescope's (Fig. 4.2.) requirements and supports are described.
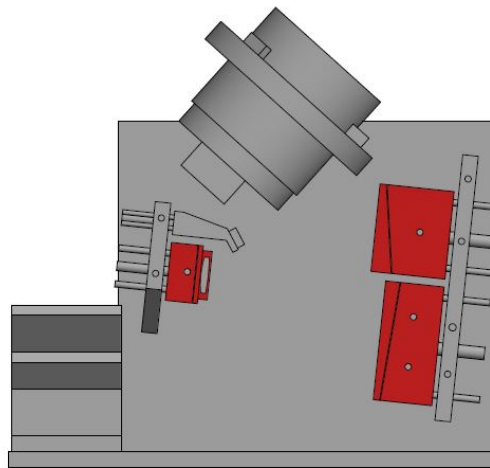
Fig. 4.2. *The TMA subsection.*

4.2.1 The TMA telescope's requirements

The TMA telescope consists of three mirrors. M1(Fig. 4.5.) and M3(Fig. 4.6.) are concave mirrors, M2 (Fig. 4.7.), instead, is a convex mirror. The next table contains the characteristics of the three TMA mirrors.

Mirror	Curvature	k
M1	467	-1.474
M3	225	+0.196
M2	141	0

Where k is the conic constant. For all the telescope mirrors the reference wavelength is 633 nm. The required distances between the mirrors are drawn in Fig. 4.8. It would be preferable to define the distances between the mirrors' vertices, to avoid possible distance variations due to the mirrors' tolerance, but in this case the reference has been chosen to be the back of M1.

During the characterization process the telescope will have to be aligned. To do so it is necessary that the three mirrors can move along the xyz directions, taking the center of M1 as a reference, and they can undergo tip-tilt rotations. So each mirror must have five DOF (Fig. 4.3.). All the TMA mirrors will be manufactured by Tecnottica srl, an Italian mirrors manufacturer.
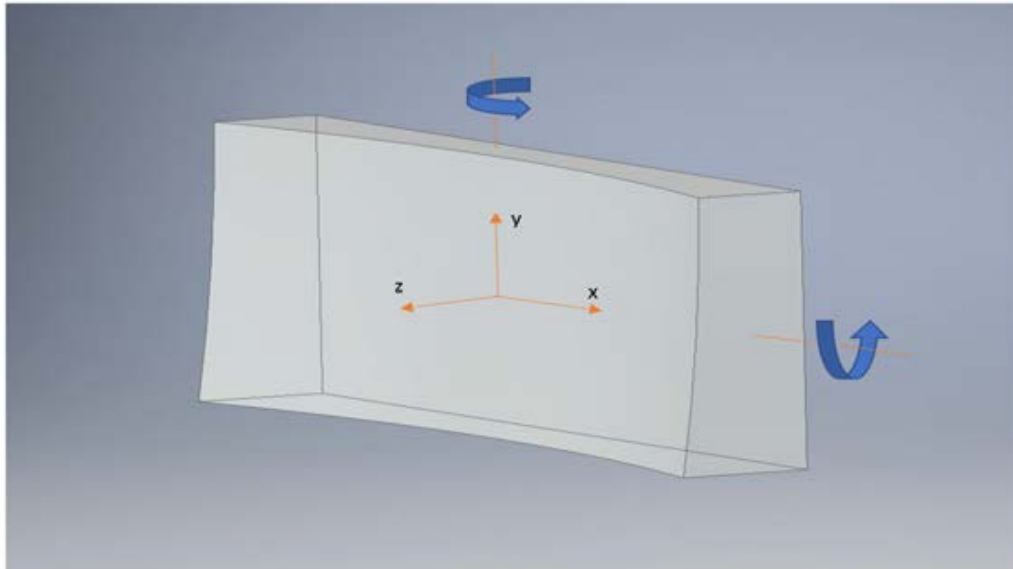
Fig. 4.3. *The TMA mirrors' degree of freedom.*

4.2.2 The TMA telescope's supports

To fulfil these requirements three different custom Al structures have been developed. The supports' shapes have been chosen, among various different ideas, because they were the ones that guaranteed the greatest rigidity of the mirrors inside the supports. Moreover, the M1 and M2 supports have been designed to simplify the fixing of the frames. Each support will be excavated so to create a cradle where the mirror is retained. The excavation depths have been designed to leave 1 mm of the mirrors out of the supports, allowing the frames to push the mirrors inside the supports.

The mirrors' nominal positions have been calculated with the supports being at a distance of 3 mm from the support walls.

The mechanisms that will guarantee the required movements are the same for the three supports. Flathead plastic grains are used to enable the movements along x-y axes during the alignment. For this purpose on every side of the supports a 1.5 mm backlash has been designed. However, the M1 and M2 topsides, and the M3 bottom side, are very close to other objects. This makes the grain impossible to access with a tool. For this reason on these sides coil springs will be used. On the back of each support four screws will be inserted. In the back center a hole is created to allow the positioning of one screw (M8 for the mirrors M1 and M3, M6 for the mirror M2) that will sustain the support and it will enable the alignment along z axis. This screw will be threaded to the wall and can be adjusted by a dedicated nut. The other three screws (M4 for all the supports) will be threaded directly on the support. To be sure the screws are fixed glue will also be used. The three screws will be positioned to form an L, this will guarantee the tip-tilt rotation. These screws will not be fixed to the wall and to allow some freedom in their movement the holes in the wall will have a backlash of 0.5 mm. Due to the extreme precision needed the hole tolerance on the support has been chosen to be 4H. To guarantee the rigidity of the mirrors inside the support they will be retained by an Al frame. This frame will push the mirror against two spring coils inserted at the base of each support guaranteeing the required stability. To be sure the mirrors will not break under the frame pressure the stress analysis on each mirror has been conducted.

Despite the alignment mechanism is the same for the three supports, due to the different mirrors weights and shapes, the supports are very different between each other. M1 and M3 are larger than M2, so the structures must be thicker. Thus the M1 (Fig. 4.9.) and M3 (Fig. 4.10.) supports thickness is 8 mm, except for the two closer sides, which are 5 mm thick. M2 (Fig. 4.11.) support is 5 mm thick on the top and bottom sides, it's thicker on the other sides because of the holes needed for the M2 frame. Even the frames are different from each other. M1 (Fig. 4.12.) and M3 (Fig. 4.13.) are both concave mirrors, thus their frames have different sizes but their shapes are similar. The frames have been designed in such a way that the support, once fixed, would have the shape of a rectangle parallelepiped. M2 (Fig. 4.14.), instead, is a convex mirror. This implies the need to use a totally different frame from the others: indeed, its shape must follow the curvature of the mirror's surface. In order to not scratch the mirror's surface the frame will lay on the mirror's surface with a 1 mm thick frame. The holes on the frame have been designed to be wider allowing the frame to move in solidarity with the mirror during the alignment process. All the frames have a central hole that will allow using a laser ray during the telescope alignment. These holes will be covered, using threaded nuts for M1 and M3 and a plastic cap for M2, once the telescope has been aligned. All the frames will be fixed to the supports with M3 screws.

The supports will be manufactured by the Asiago Observatory mechanic workshop. The frames will instead be printed at the CISAS laboratory.

4.2.3 The telescope's mirrors stress analysis

To verify that the frames do not cause excessive deformation on the mirrors, a stress analysis was conducted on each telescope mirror. First the 3D mirror file was reproduced and then the deformations caused by the frames were calculated using a finite element analysis. The worst case scenario in which the springs coil are totally compressed was considered. The study was carried out by imposing four acting forces, one on each vertex of the mirror surface. The mirror base was imposed to be fixed.

The maximum tolerated deformation is defined as $\lambda/20$, where $\lambda = 630$ nm is the standard HeNe laser wavelength. The following table shows the maximum tolerated compressive load.

Mirror	Maximum load (N)	Maximum displacement (nm)
M1	6	30
M3	3	33
M2	4	32

The results show that on each vertex a load of about 0.5 kg can be applied. However, the deformation only affects the part close to the summits. The analysis has therefore ensured that the frames will not cause a deformation harmful to the mirrors. All the analysis were made using the Inventor software.
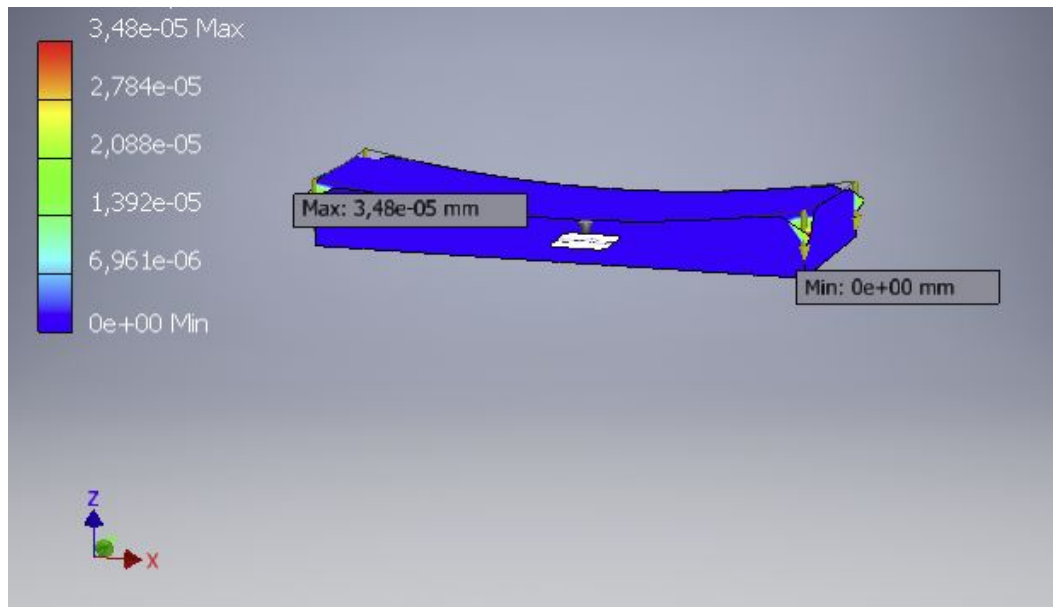
Fig. 4.4. *Compression loads on M1.*
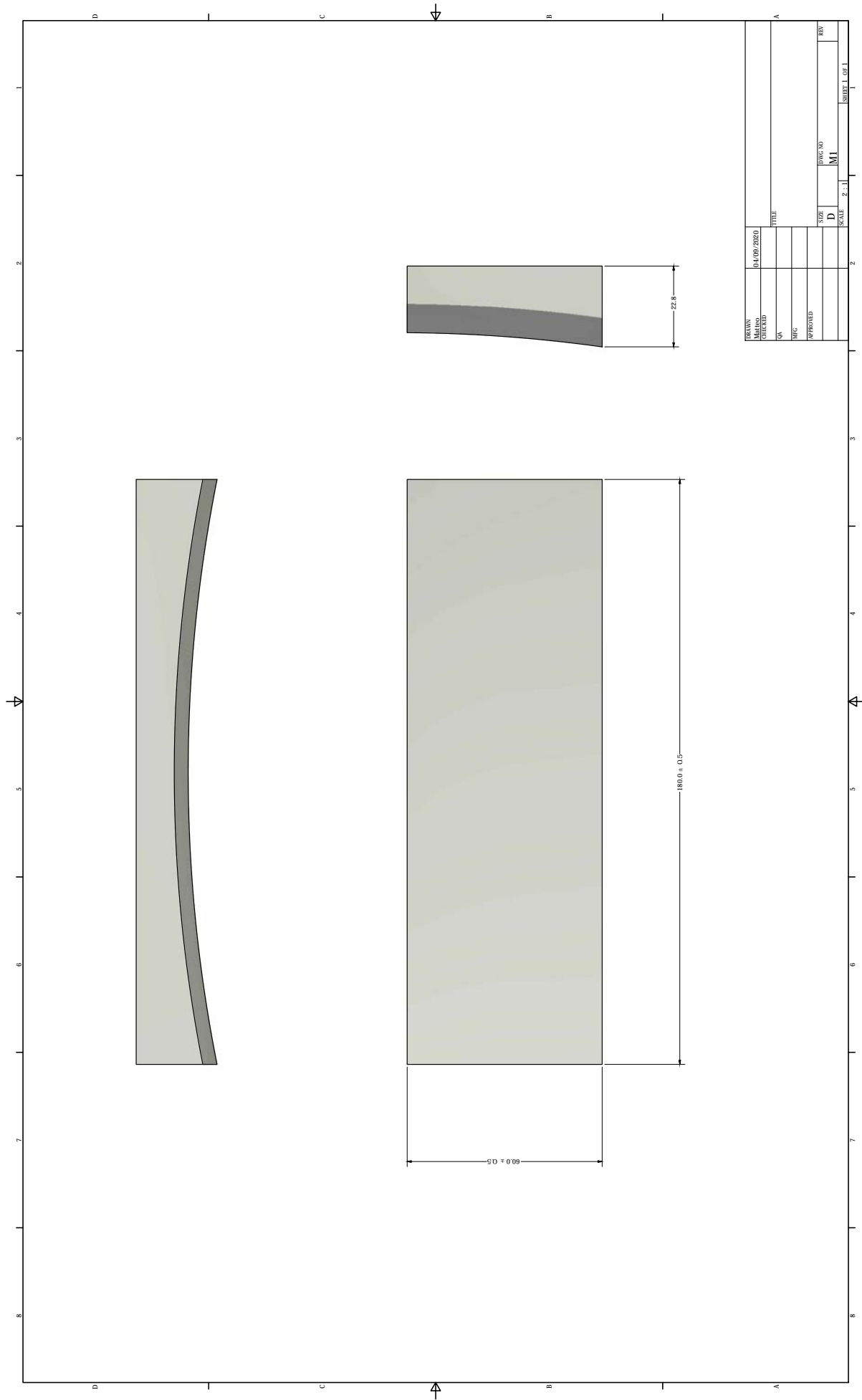
Fig. 4.5. *The M1*

Fig. 4.6. *The M3*
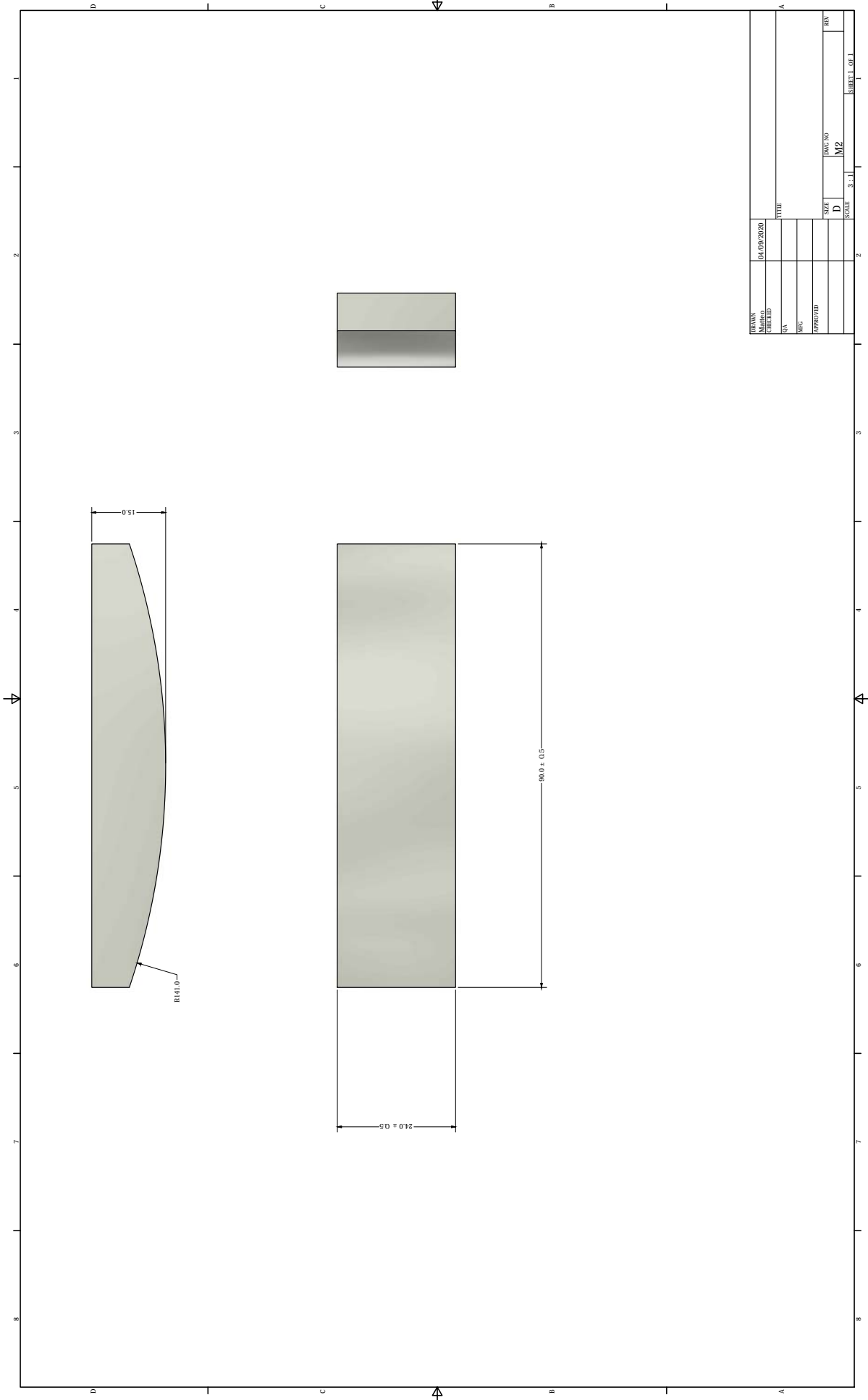
Fig. 4.7. *The M2*

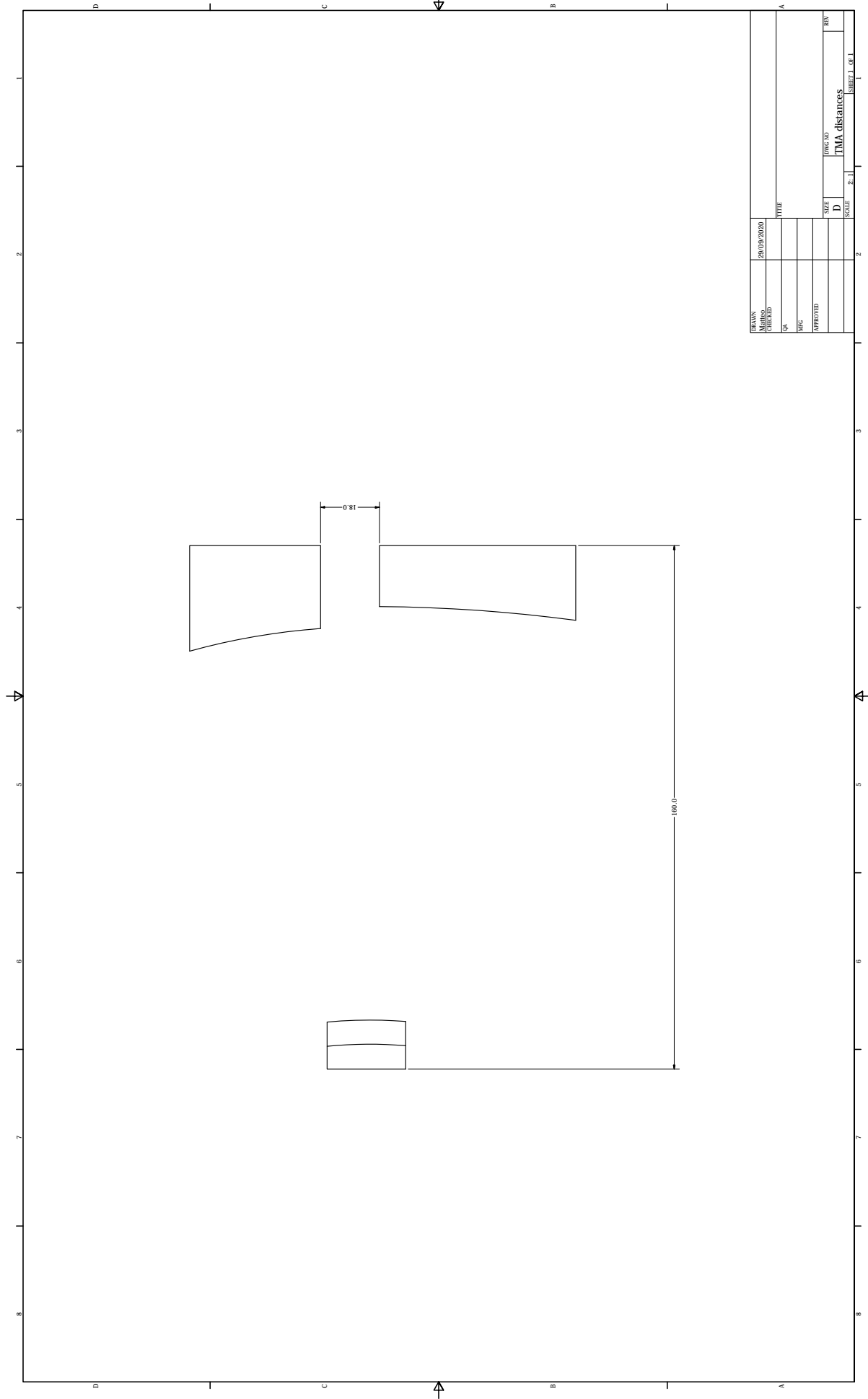Dimensions visible on drawing:
- 15.0
- R141.0
- 90.0 ± 0.5
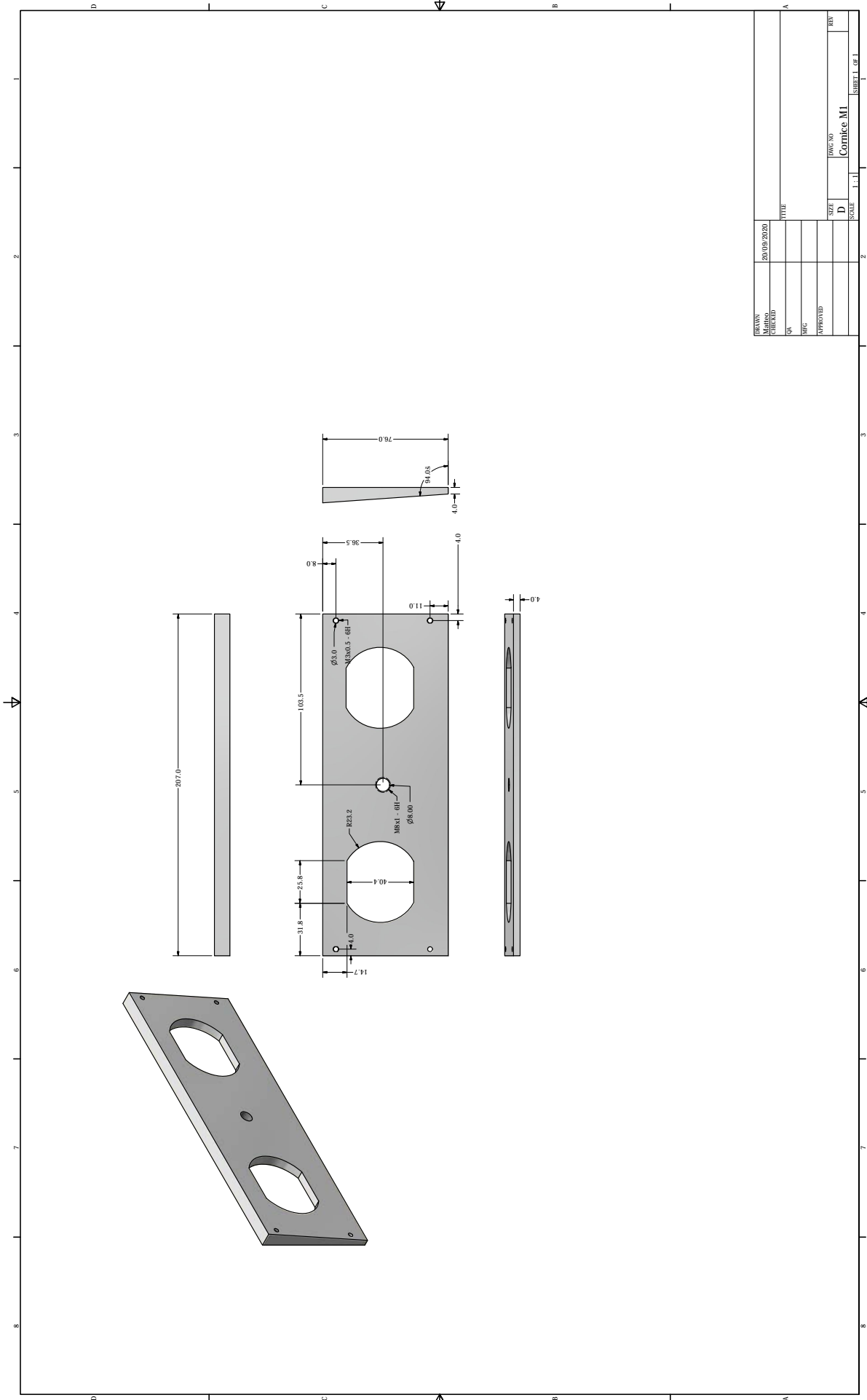- 24.0 ± 0.5

Fig. 4.8. *TMA mirrors distances*

Fig. 4.9. *The M1 Support*

Fig. 4.10. *The M3 Support*

Fig. 4.11. *The M2 Support*

Fig. 4.12. *The M1*

4.0

80°

4.0

56.0

11.0

92.5

M8x0.5 - 6H

Ø3.00

Ø10.00

M10x1 - 6H

185.0

R14.15

27.0

28.3

33.1

4.0

8.0

18.2

29.5

Fig. 4.13. *The M3*

Fig. 4.14. *The M2*

4.3 The Folding Mirror (FM)

In this section the FM's (Fig. 4.15.) requirements and support are described.
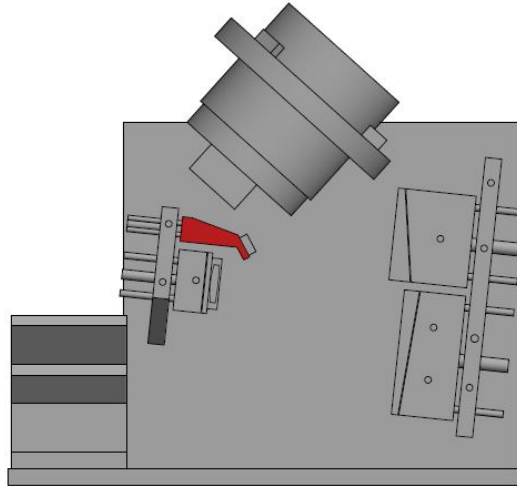

Fig. 4.15. *The FM subsection.*

4.3.1 The FM's requirements

The folding mirror (Fig. 4.17.) is a tiny plane mirror used to place the telescope focal plane in a convenient position. Thus, its position defines also the spectrometer position. The angle of the FM and its position relative to M3 can be chosen in a wide range of possibilities. In the choice of the FM's optimal position the following constraints have been considered (Fig. 4.16.):

a) the distance between the FM's support and the M2-M3 ray must be at least 4 mm;

b) the distance between the FM's support and M2's support must be at least 5 mm;

c) the FM's angle must allow a distance between the FM's support and the detector of at least 10 mm;

d) the FM's angle must allow a distance between the spectrometer's support and the M3-FM ray of at least 10 mm.

To fulfil these constraints an angle of 0.6 rad with respect to M3 and a distance of 127 mm from M3 have been chosen.
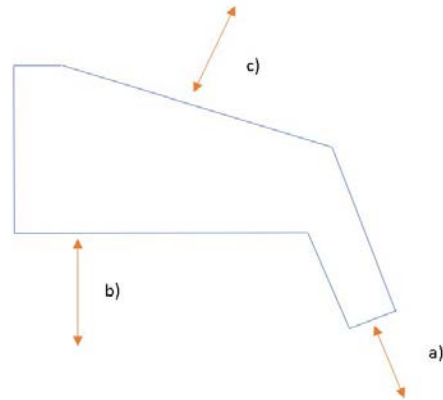
Fig. 4.16. *The constraints on the FM's position choice.*

4.3.2 The FM's support

During the alignment process even the FM's position must be corrected. As for the three TMA mirrors' supports, a four screws configuration has been chosen. The three smaller screws, arranged in L configuration, guarantee the tip-tilt rotation. The bigger central screw guarantees the movement along z axis and sustains the support. As for the TMA supports the required hole tolerance is 4H because of the great precision required. The plane mirror will be glued to the support, without the possibility of moving it along x-y axes. Even without this possibility the other DOFs of the assembly should guarantee a simpler alignment of the telescope with the spectrometer.

The design of the back of the FM's support (Fig. 4.18.) was influenced by the need to leave enough space for the nuts and the screws' holes.
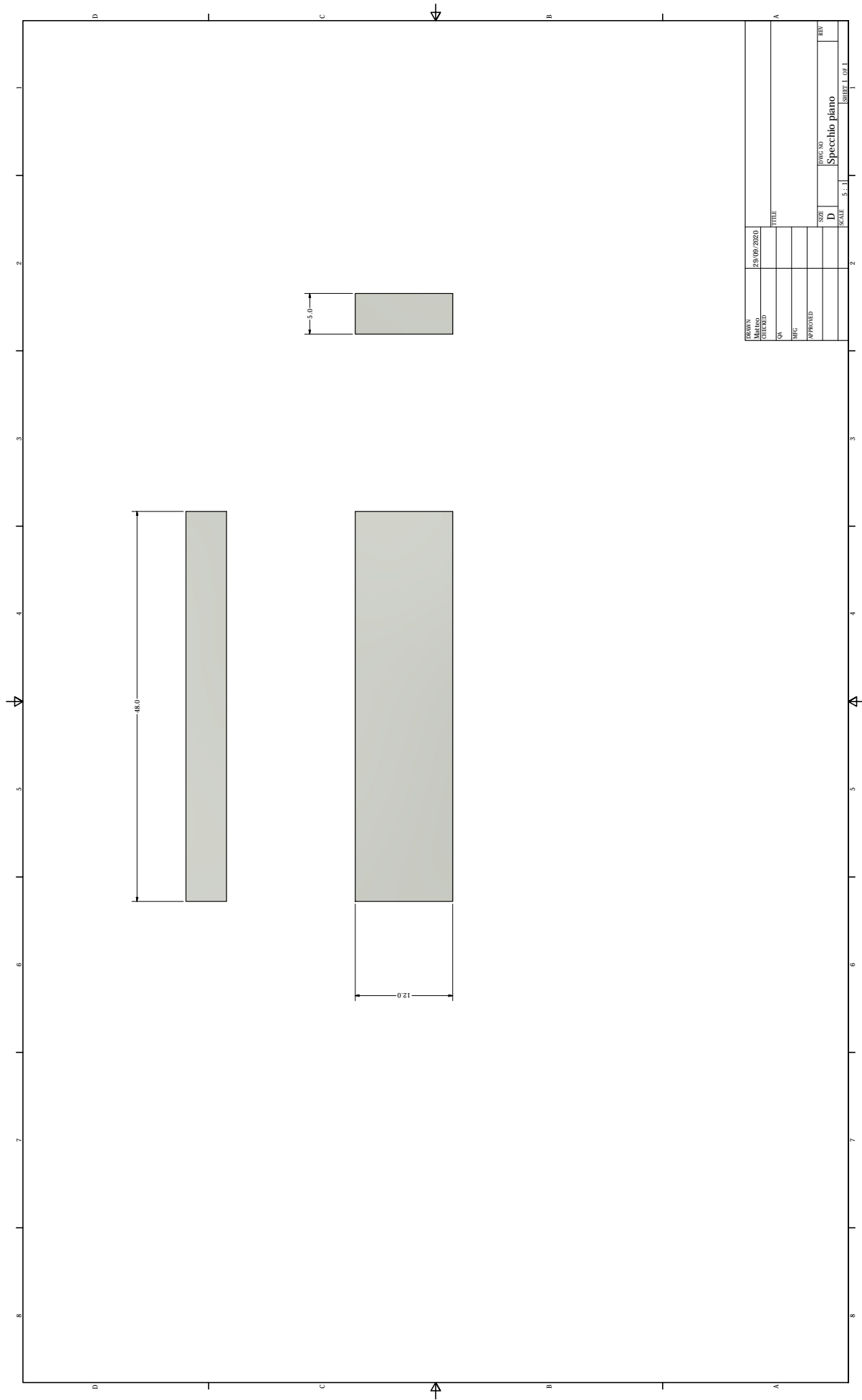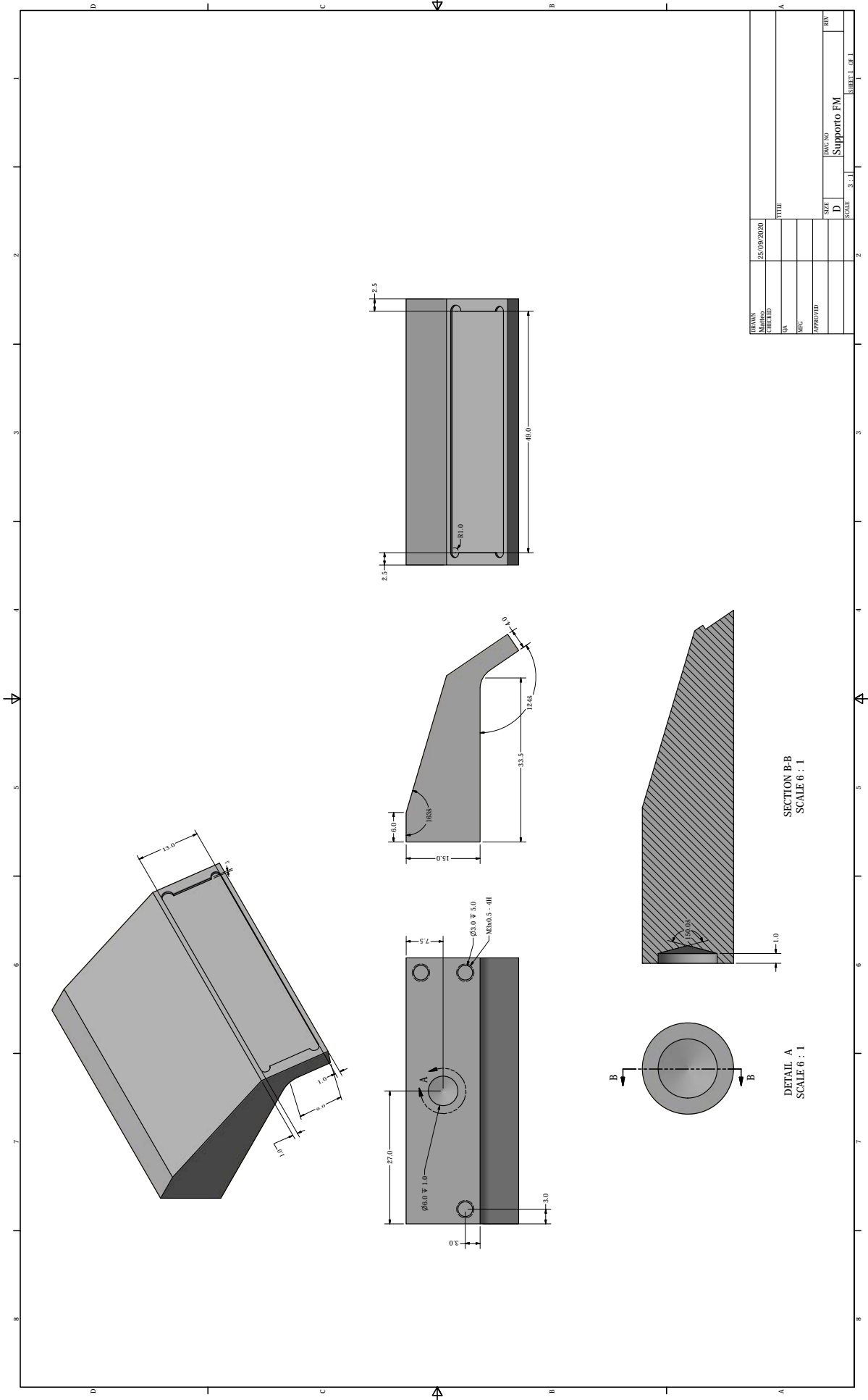
Fig. 4.17. *The FM*

Fig. 4.18. *The FM's support*

4.4 The Spectrometer

In this section the spectrometer's (Fig. 4.19.) requirements and support are described.
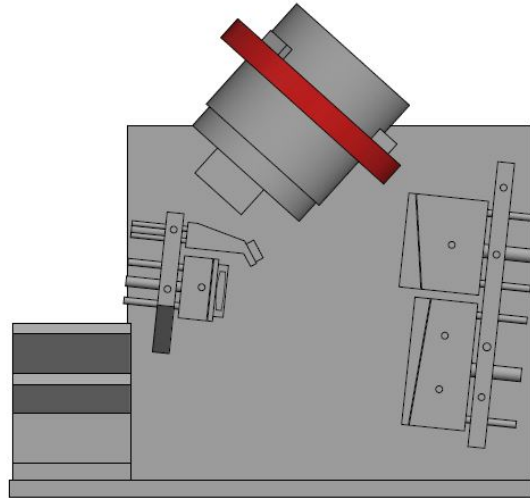

Fig. 4.19. *The spectrometer subsection.*

4.4.1 The spectrometer's requirements

The spectrometer consists of five different lenses and a grating. All these components will be inserted in a cylinder that will be developed by the lenses manufacturer. In Fig. 4.21. are represented the required sizes of the cylinder. The three outgoing rectangles will be necessary to fix the cylinder to its support. The alignment of the telescope with the spectrometer is one of the main challenges in the development of the HYPSOS prototype. For this reason the spectrometer must be able to be moved with the required DOFs (Fig. 4.20.).
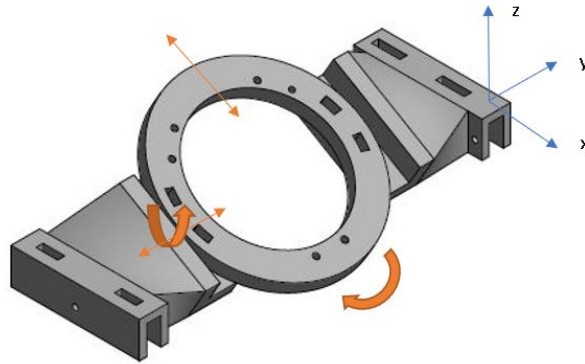
Fig. 4.20. *The spectrometer's required DOFs.*

4.4.2 The spectrometer's support

The cylinder's supports consists of three pieces. The cylinder will be fixed to a ring (Fig. 4.22.) fixed to the lateral walls by two supports. These supports (Fig 4.23.), one for side, will be fixed to the lateral walls by five M3 screws. These structures have been designed to be long enough to assure the required assembly stability. In fact, the bench will rotate to simulate the different stereo angle, so the structure must be as rigid as possible to avoid slit's vibrations, which would contaminate the data acquired. The structures supporting the ring have two rectangular holes on the top side and three screws on the lateral sides, to allow the alignment along the x-y axes. The desired alignment along the z axis can be obtained by using shims. The alignment mechanism for the cylinder is the same as for the TMA supports. In total six screws are used. Three will be threaded to the cylinder, allowing to pull the cylinder against the ring, three other will be threaded to the ring, allowing to push away the cylinder from the ring. The ring will be fixed to the two supports by two M4 screws on each side. The holes in the ring are not circular to allow the ring rotation. In these ways all the required DOFs are guaranteed. Due to their particular shapes the ring's supports will be printed at the CISAS laboratory, the ring, instead, will be manufactured at the mechanic workshop of the Asiago Observatory.
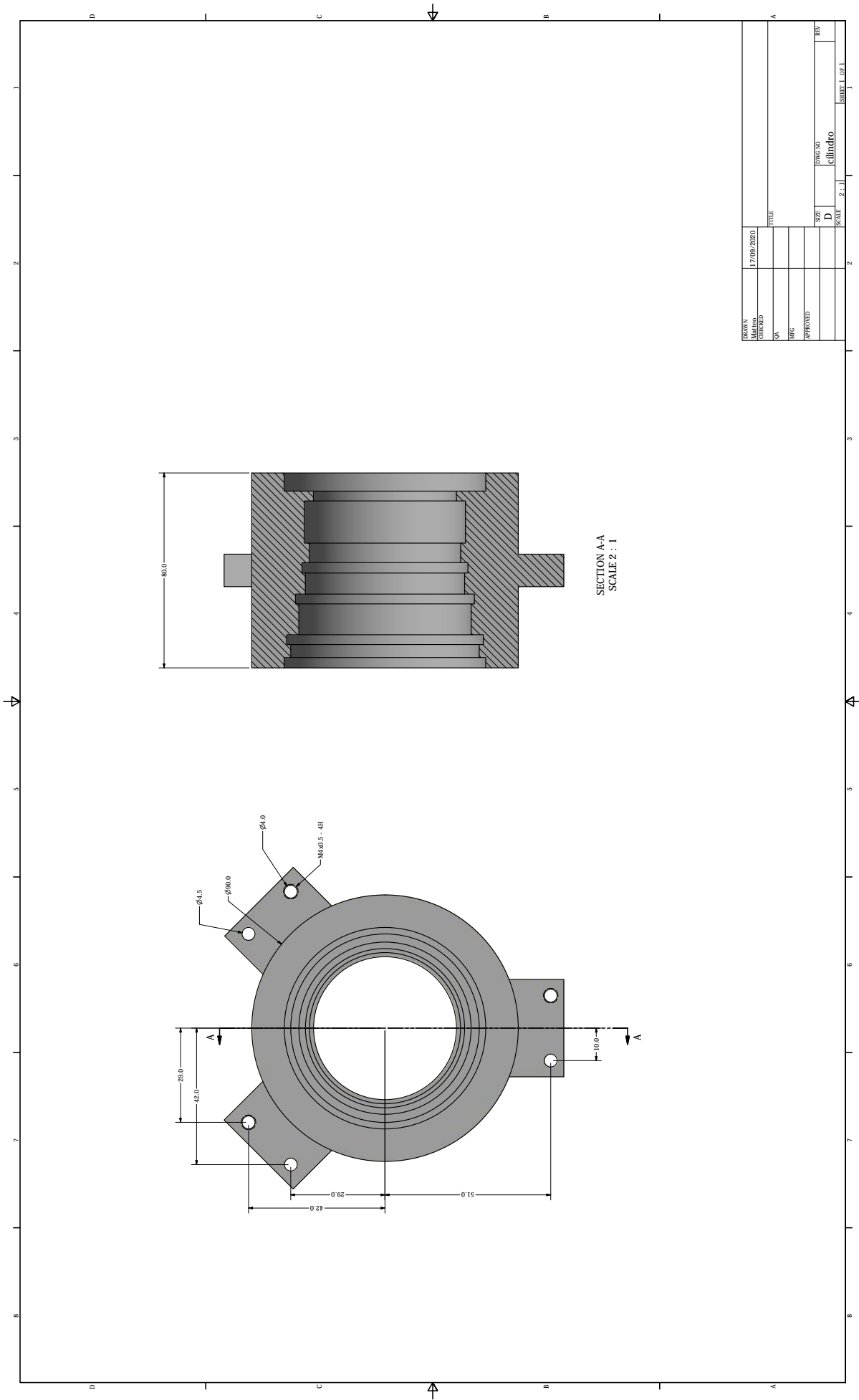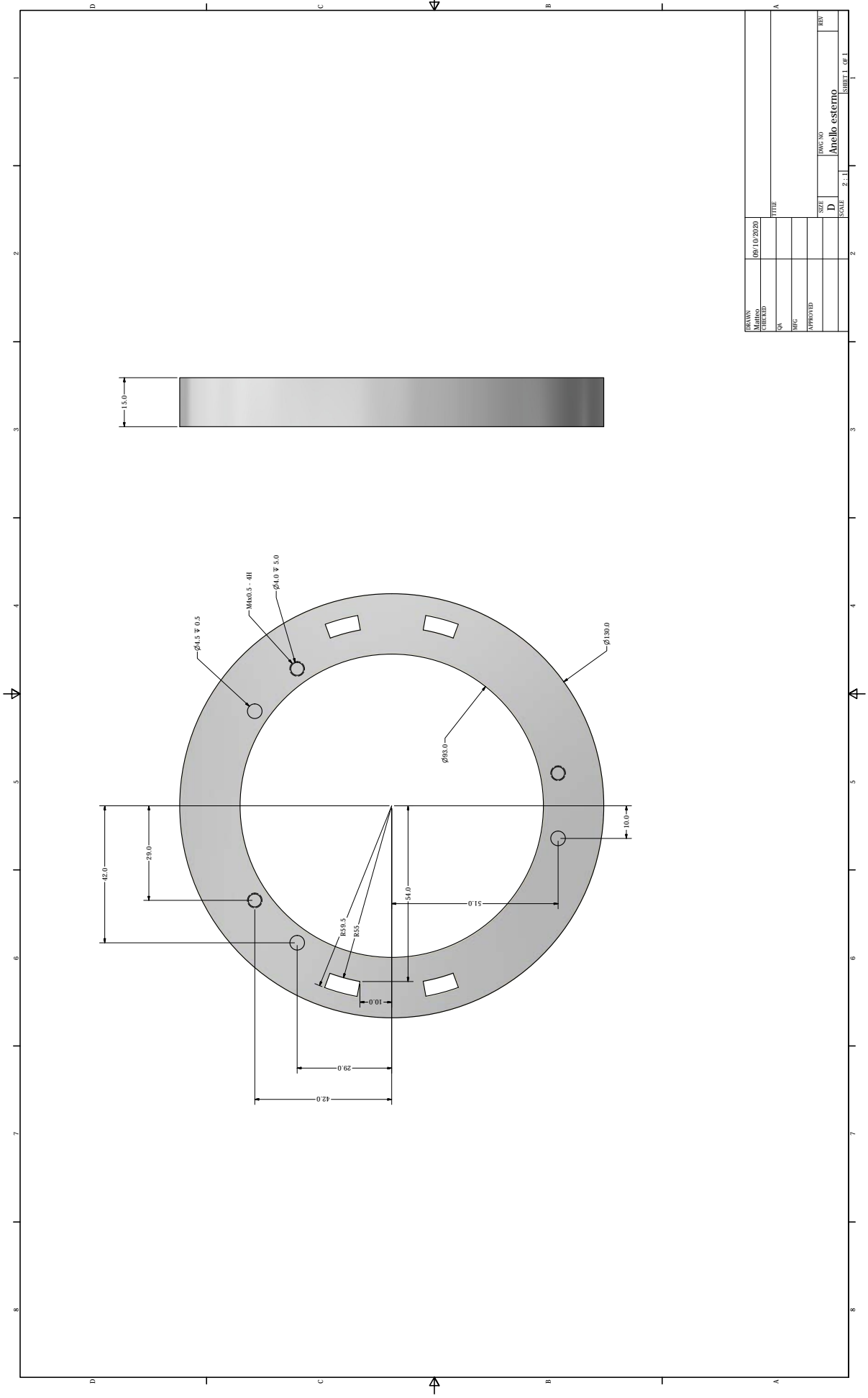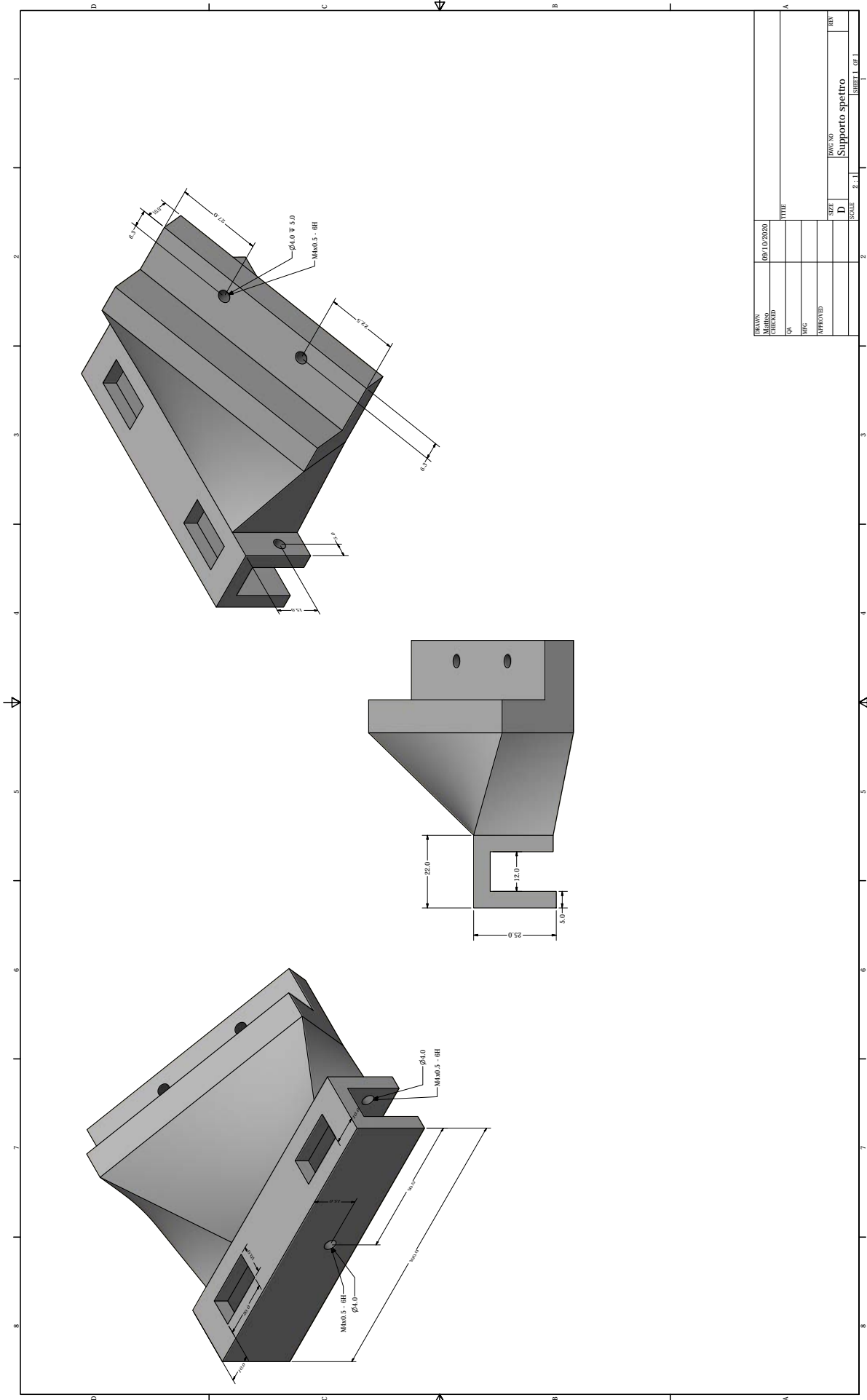
Fig. 4.21. *The cylinder's required sizes*

Fig. 4.22. *The ring*

Fig. 4.23. *The ring's support*

4.5 The slit-detector assembly (SDA)

In this section the SDA (Fig. 4.24.) requirements and support are investigated.
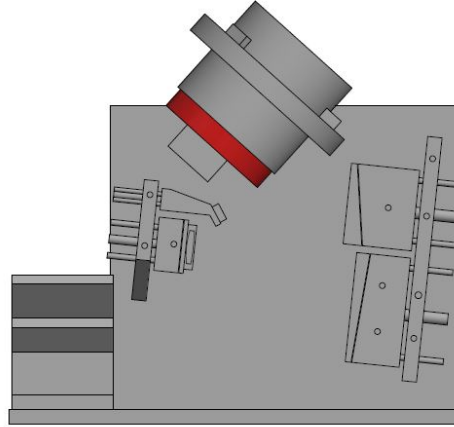
Fig. 4.24. *The SDA's subsection.*

4.5.1 The SDA's requirements

The SDA alignment, containing the slit and the detector, is of capital importance. For this reason it has been chosen to insert the two objects in a single rigid structure that will be fixed to the spectrometer's cylinder. This is possible because the slit and detector's required positions (Fig. 4.25.) allow creating a structure without any crossing problems. Moreover this kind of support will reduce the stray light that can enter inside the spectrometer.
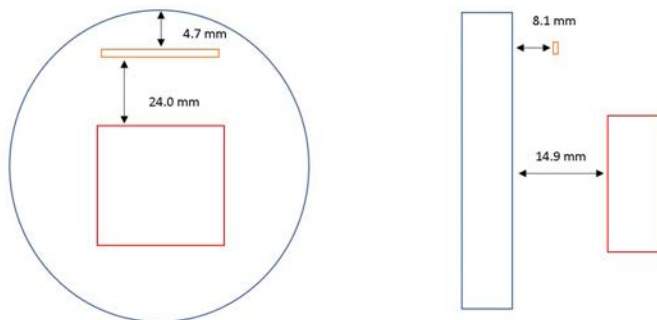
Fig. 4.25. *The slit and detector required distances (not in scale).*

In this prototype a board-level detector will be used. To avoid electro static discharge that would definitely damaged the detector, the support material must be non-conductive. For this reason the support will be printed at CISAS laboratory.

4.5.2 The SDA's support

The support (Fig. 4.26.) is a circular structure with two holes inside. One will allow entering the light from the telescope, the other is used to fix the detector. The slit will be fixed by a frame on a rectangular support (Fig. 4.27.) that will be fixed to the SDA support. Once the slit and the detector have been inserted in the structure they can still be aligned by using shims. The overall structure will be fixed to the spectrometer cylinder by four M5 screws.
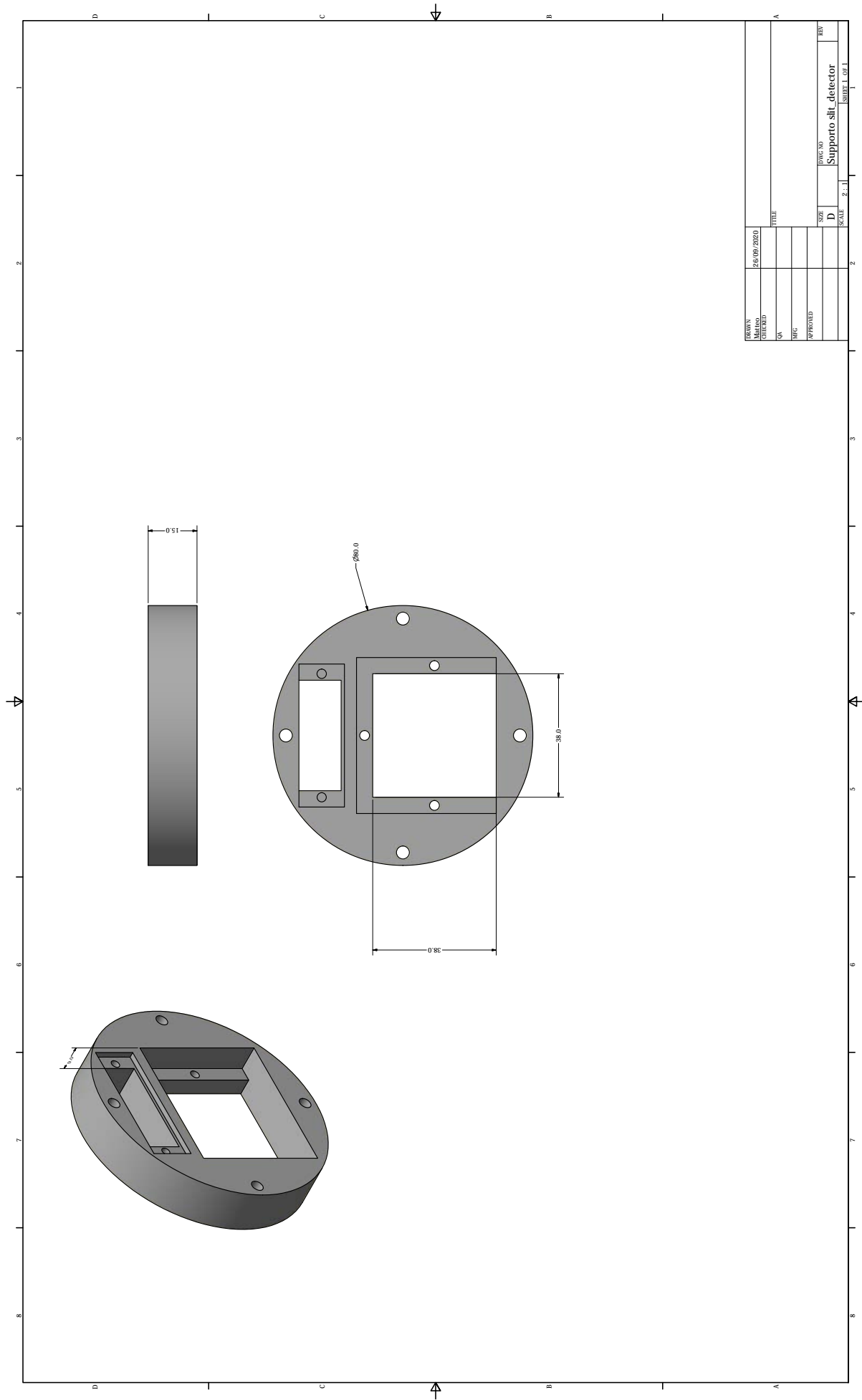
Fig. 4.26. *The SDA's support*

Ø80.0

15.0

38.0

38.0

SECTION A-A
SCALE 5 : 1

44.0

DRAWN Matteo 26/09/2020
CHECKED
QA
MFG
APPROVED

TITLE

DWG NO
Rettangolo slit

SIZE D
SCALE 5 : 1

REV

SHEET 1 OF 1
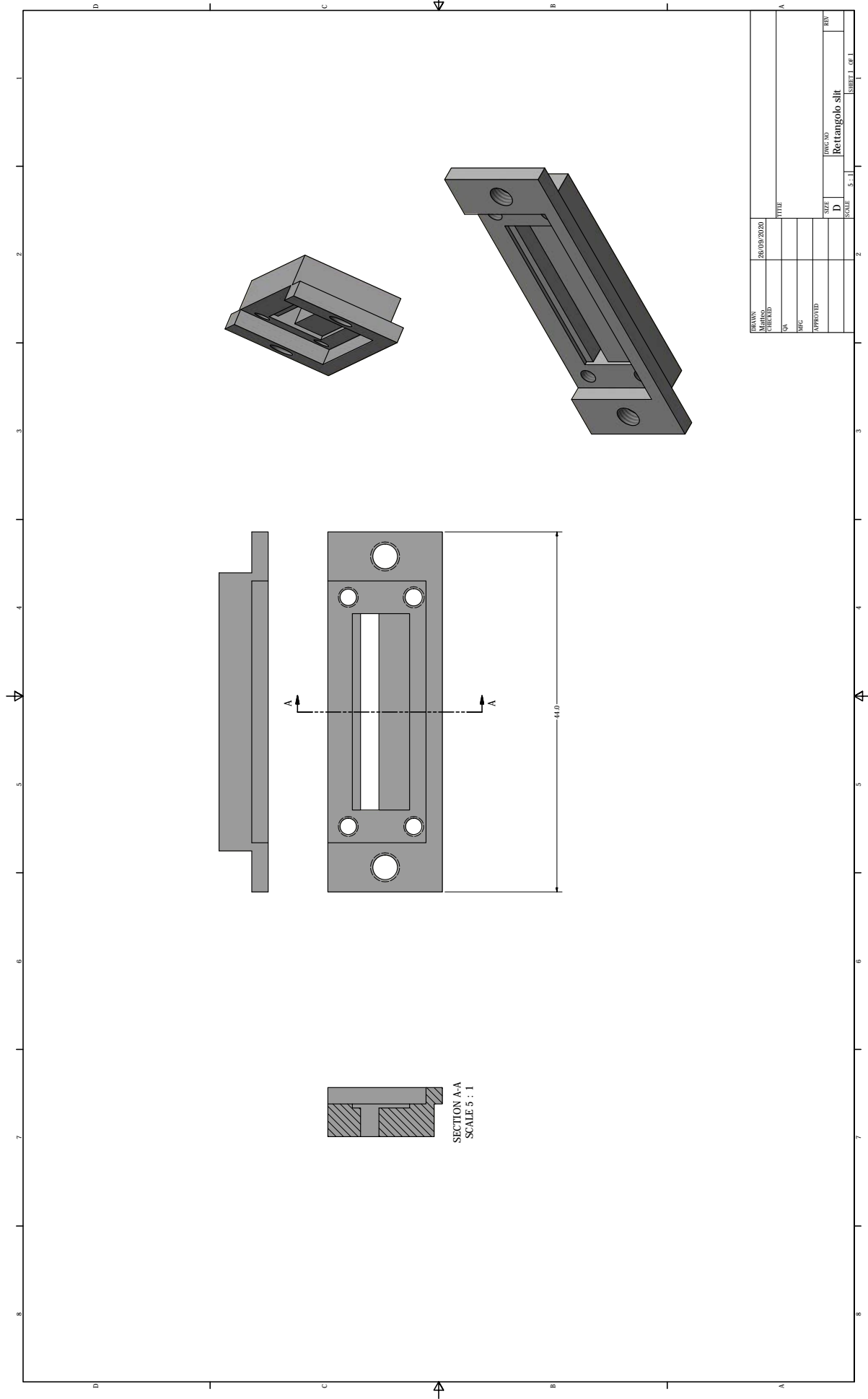
Fig. 4.27. *The slit's support*

4.6 The rotators

In this section the rotators' (Fig. 4.28.) requirements and supports are investigated.
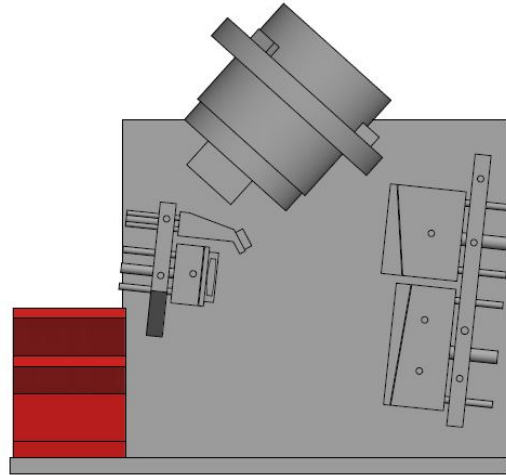
Fig. 4.28. *The rotators subsection.*

4.6.1 The rotators' requirements

The rotators consist of two Pechan prisms. These are used to rotate the incoming light ray by 90° in order to have the two images on the same plane. To obtain this rotation the two prisms must be tilted by 45° with respect to the optical bench's base. Every small deviation from this angle causes a misalignment of the focal plane of the two images. Thus it's very important that the two prisms are rigidly fixed and correctly tilted.

4.6.2 The rotators' support

To fix the Pechan prisms at the right angle a two pieces support has been designed. Its base (Fig. 4.29.), fixed at the optical bench by four M5 screws, assure the required 45° angle, while the U structure (Fig. 4.30.) allows fixing the Pechan prism position with four M3 screws. The two support's parts are fixed between each other by four M5 screws.
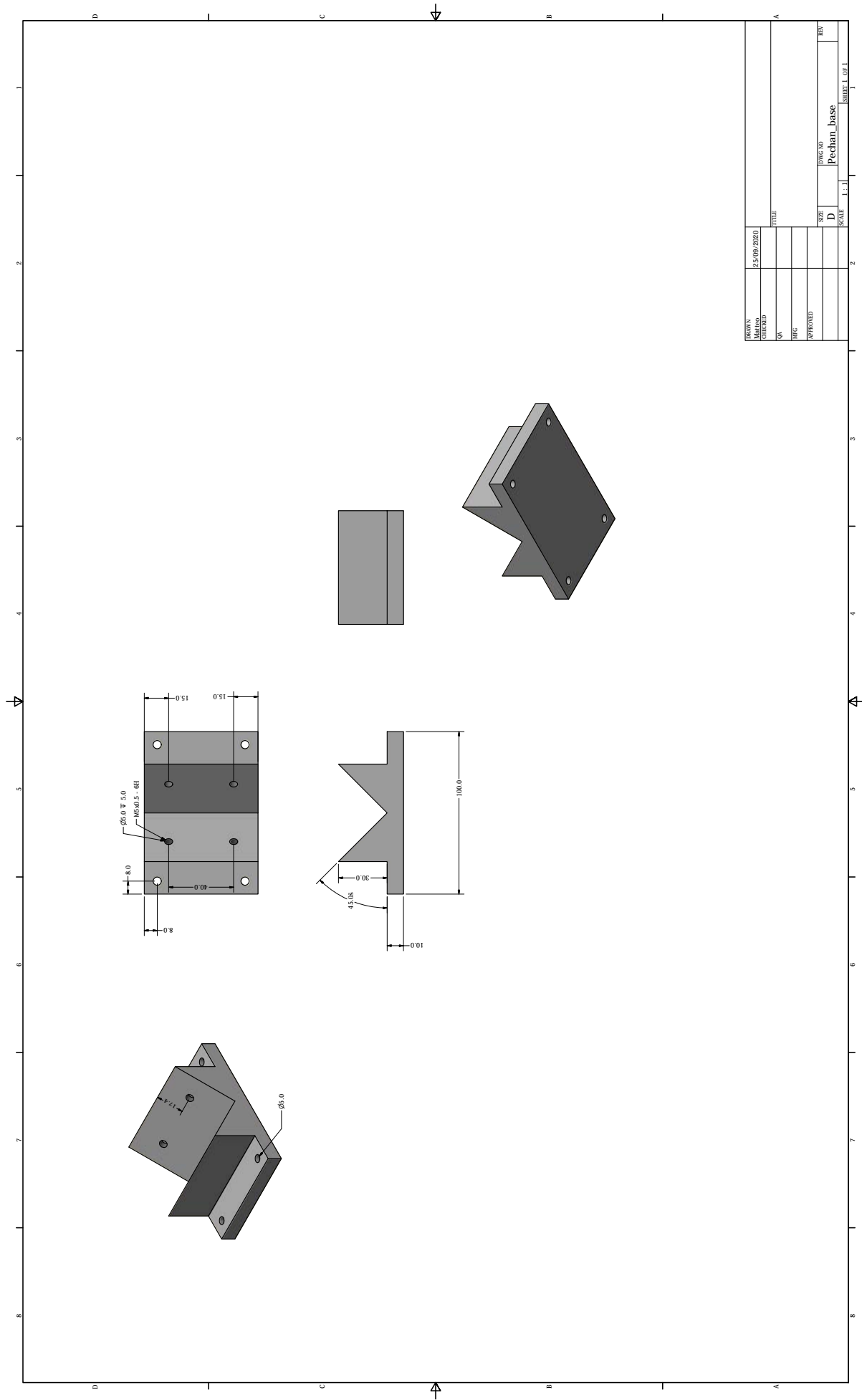
Fig. 4.29. *The rotator's base support*
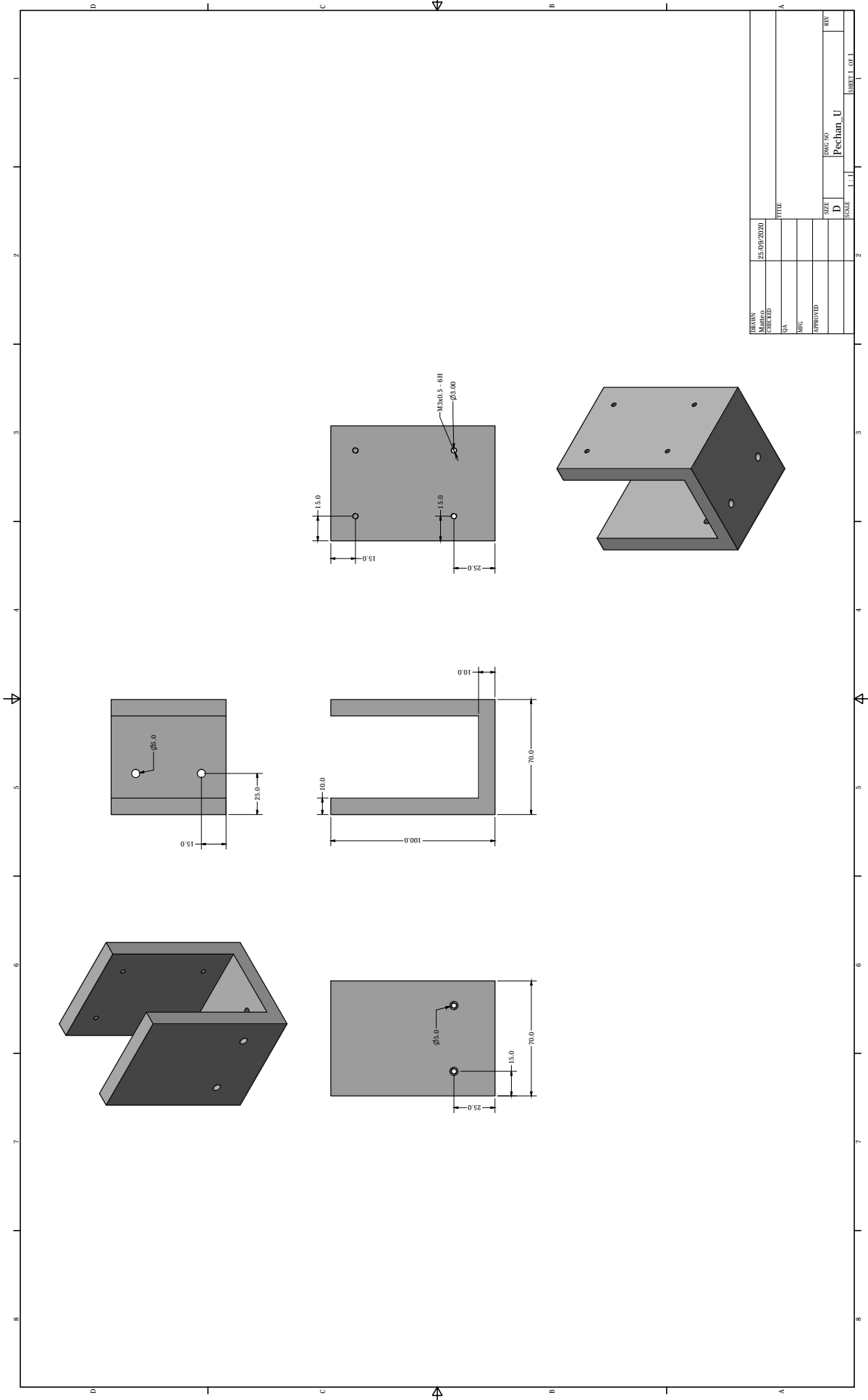
15.0
15.0
Ø5.0 ▽ 5.0
M5x0.5 - 6H
8.0
40.0
8.0

100.0
30.0
45.0°
10.0

Ø17.4
Ø5.0

Fig. 4.30. *The rotator's structure support*

4.7 The walls

In this section the walls (Fig. 4.31.) that make up the optical bench are described.
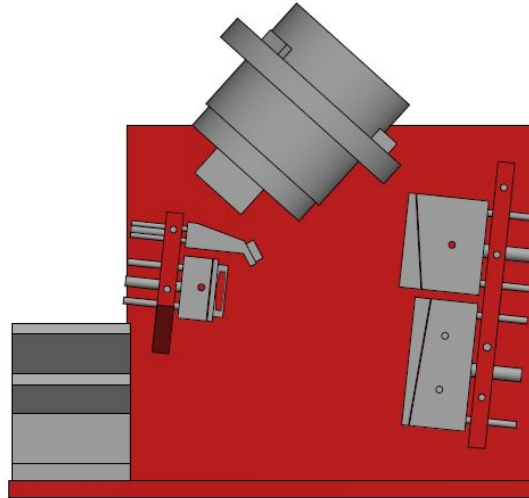
Fig. 4.31. *The walls subsection.*

4.7.1 The walls' structure

The walls have to be thick enough to sustain the optical bench overall weight. It has been chosen that the base thickness should be 15 mm. All the other walls are 10 mm thick. In the optical design the telescope is tilted by 6° with respect to the incoming ray. To simplify the holes' design it has been chosen to tilt the walls that sustain the telescope mirrors (Fig. 4.32. and Fig. 4.33). These will be fixed to the lateral walls (Fig. 4.34.) that will sustain them. The M2 and M1 walls inclination is fundamental because it will define the relative positions between the mirrors. For this reason the tolerance on the holes' positions is 0.1 mm. The lateral walls, in turn, will be fixed to the optical bench base (Fig. 4.35.). To access the grains during the alignment process three holes on the lateral walls have been designed. During the characterization phase the base will be fixed to a rotator, allowing to simulate various incidence angles. To reduce stray light inside the prototype some internal baffles have been designed.

The bench assembly procedure will be as follows:

1. the base will be slightly fixed to the side walls;

2. the assembly will be fixed to the rotator;

3. the optical components, M1, M2, M3, and the FM, will be mounted on the dedicated two walls;

4. the M2 and M1 walls will be slightly fixed to the side walls;

5. the lower and side screws will be simultaneously tightened;

6. the telescope will be aligned;

7. the two Pechan prisms will be inserted;

8. the spectrometer will be inserted and aligned with the telescope.
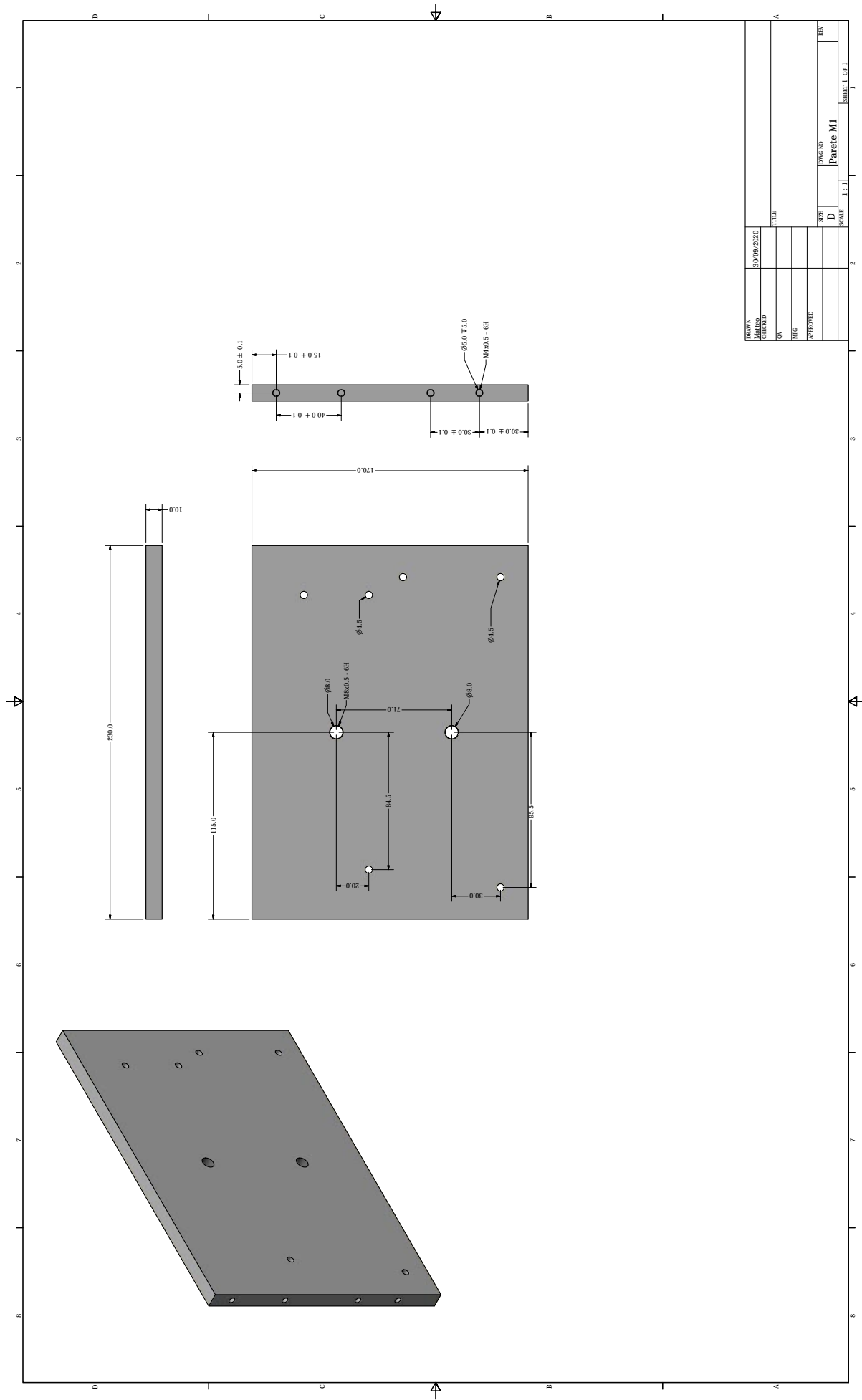
Fig. 4.32. *The M1 wall*
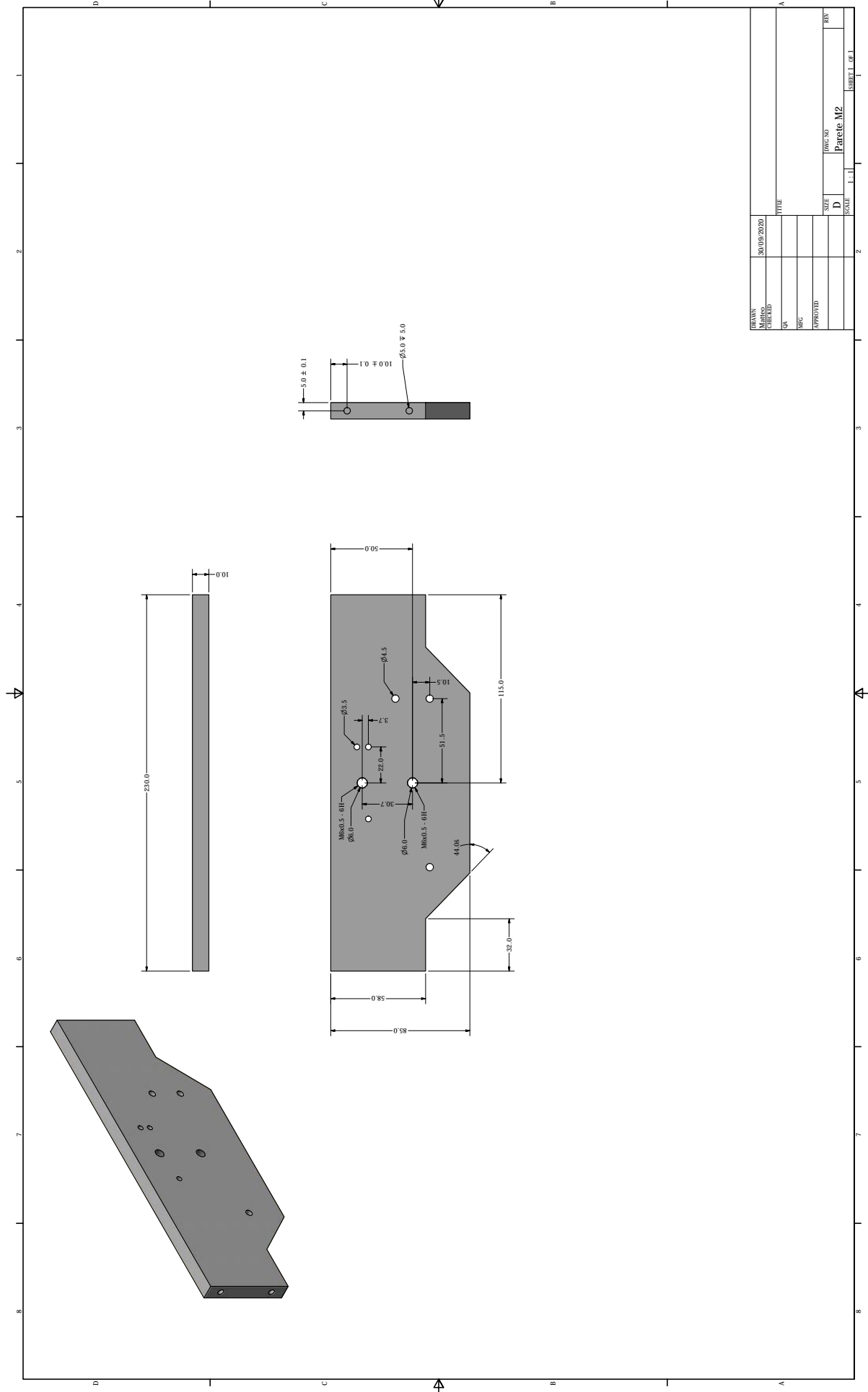
Fig. 4.33. *The M2 wall*
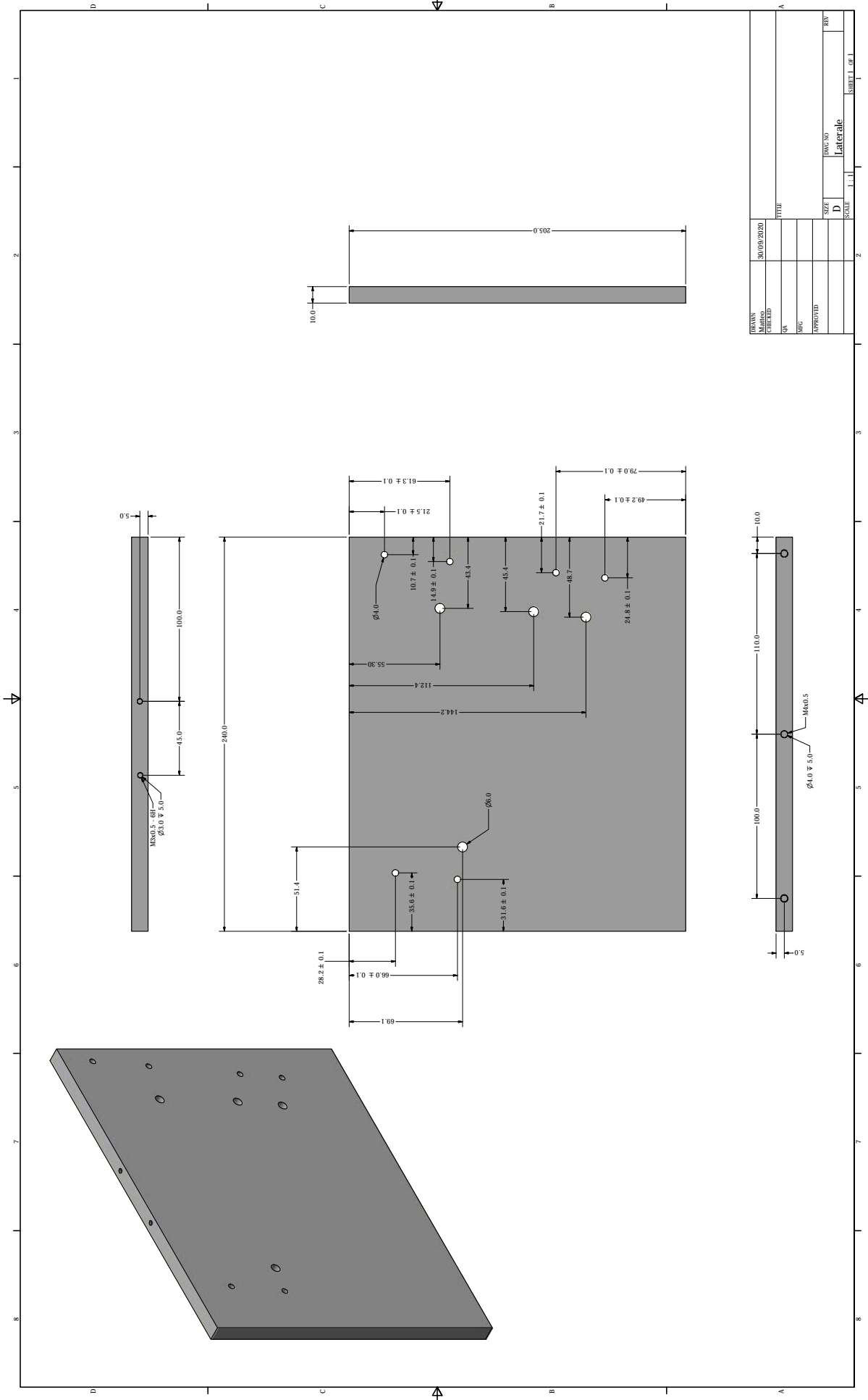
Fig. 4.34. *The lateral wall*
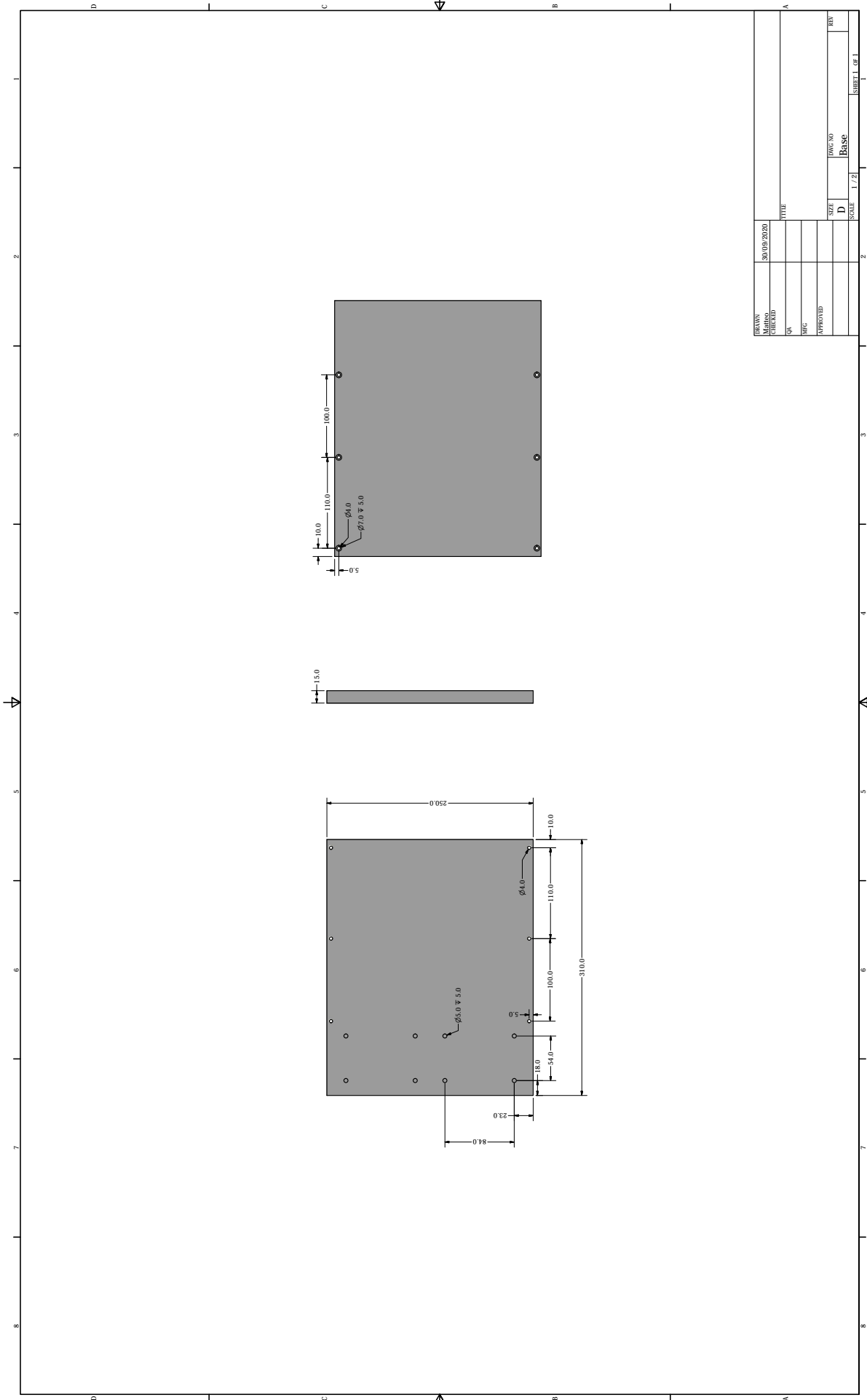
Fig. 4.35. *The optical bench base*

Conclusions

In this thesis the work done during the last six months in the design of the HYPSOS optical bench has been described. The optical configuration of some components has yet to be frozen, so some technical drawings, described in this dissertation, may not be the final ones.

It is expected to finish a first model, printing all the main components at CISAS, by the end of November; while the actual bench will have to be assembled by the end of January, the date of arrival of the telescope mirrors.

The design of innovative and original components turned out to be a very stimulating work: the space is very limited and the alignment mechanisms have to be easily accessible during the prototype characterization. Ultimately the designed bench can be enclosed in a solid with dimensions 230x310x250 mm^3, providing all the degrees of freedom required by the various components for the alignment process. All the alignment procedures can be done with the prototype being closed.

To complete this dissertation the candidate learn to use Inventor software and, thanks to the instructive advices and patience of Prof. Naletto, has learned a lot about the optomechanical design process.

I'd like to conclude this dissertation with a quote reported by Prof. Naletto: "*L'ottica è l'arte dei supporti*". Its mean is that optics is the art of the supports. I will always remember it and, hopefully, use in my future career.

References

[1] Feynman, Richard P. *"The Feynman Lectures on Physics"*, Addison-Wesley (1963).

[2] Hecht, Eugene. *"Optics"*, Addison Wesley (1987).

[3] C.Re, R.Roncella, G.Forlani, G.Cremonese, G.Naletto, *"Evaluation of an area-based matching algorithm with advanced shape models"*, International Archives of the Photogrammetry, Remote Sensing and Spatial Information Sciences.

[4] G. Naletto, M. Cesaro, A. Albasini, G. Cremonese, V. Da Deppo, G. Forlani, C. Re, R. Roncella, G. Salemi, and E. Simioni *"Innovative optical setup for testing a stereo camera for space applications"*, Proc. SPIE 8442, Space Telescopes and Instrumentation 2012: Optical, Infrared, and Millimeter Wave, 84421M (21 September 2012);

[5] E. Flamini, et al. *"SIMBIO-SYS: the spectrometer and imagers integrated observatory system for the BepiColombo planetary orbiter"*, Planet. Space Sci. 58, 125–143 (2010).

[6] F. Capaccioni, M. C. De Sanctis, G. Piccioni, E. Flamini, S. Debei, and the SYMBIOSYS International Team, *"VIHI: the Visible and Infrared Hyperspectral Imager channel of the SIMBIO-SYS instrument for the BepiColombo mission to Mercury"*, in American Astronomical Society/Division for Planetary Sciences Meeting Abstracts (2005), Vol. 37.

[7] V. Da Deppo, G. Naletto, G. Cremonese, L. Calamai, S. Debei, and E. Flamini, *"A novel optical design for the stereo channel of the imaging system SIMBIOSYS for the BepiColombo ESA mission"*, in Proceedings of the 7th International Conference on Space Optics (2008), pp. 14–17.

[8] Patent n° 102016000097439.

Appendix A

The refraction index

In the first chapter the refraction index has been defined as the ratio between the wave phase speed in the vacuum compared to the wave velocity in a generic medium.
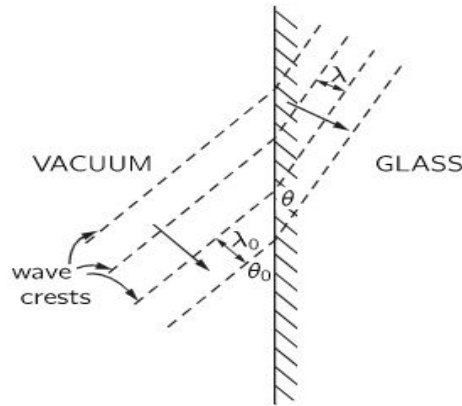
Fig. A.1. *Interaction glass vacuum.*

In figure A.1. are represented several successive crests of an electric wave which arrives from a vacuum onto the surface of a block of glass. The arrow perpendicular to the wave crests indicates the direction of travel of the wave. Now all oscillations in the wave must have the same frequency. This means that the wave crests for the waves on both sides of the surface must have the same spacing along the surface because they must travel together. The shortest distance between crests of the wave is the wavelength. On the vacuum side it is $\lambda_0 = 2\pi c/\omega$, and on the other side it is $\lambda = 2\pi v/\omega$ or $2\pi c/\omega n$, if $v = c/n$ is the velocity of the wave. From the figure you can see that the only way for the waves to fit properly at the boundary is for the waves in the material to be travelling at a different angle with respect to the surface. The purpose of this appendix is to understand how the index of refraction term could come about. To do so it is assumed that the total electric field in any physical circumstance can always be represented by the sum of the fields from all the charges in the universe and that the field from a single charge is given by its acceleration evaluated with retardation at the speed c.

Consider now the very simple case in which an external source S is placed a large distance away from a thin plate of transparent material, say glass. The field at point P, at a large distance on the opposite side of the plate, can be written as:

$$E = \sum_{i=1}^{n} E_i \tag{A.1}$$

or

$$E = E_s + \sum_{j=1}^{n-1} E_j, \tag{A.2}$$

where E_s is the field due to the source alone and would be precisely the field at P if there were no material present. If there are any other moving charges the field at P would be different from E_s. When the electric field of the source acts on the atoms of the glass it drives the electrons up and down. These electrons become new radiators related to the source S. So the total field obtained is not just the field of the source S, but it is modified by the additional contribution from the other moving charges. In this simple case is considered a material in which the total field is not modified very much by the motion of the other charges. That corresponds to a material in which the index of refraction is very close to 1, which will happen, for example, if the density of the atoms is very low. If the plate did not affect the total field, the field of a wave travelling to the right, along the z-axis, would be

$$E_s = E_0 e^{i\omega\left(t-\frac{z}{c}\right)}. \tag{A.3}$$

Let us call the thickness of the plate Δz. If the plate were not there the wave would travel the distance Δz in the time $\Delta z/c$. But if it appears to travel at the speed c/n then it should take the additional time $\Delta t = (n-1)\Delta z/c$. After that, it would continue to travel at the speed c again. You can take into account the extra delay in getting through the plate by replacing t in Eq. (4.3) by $(t - \Delta t)$. Hence the wave after insertion of the plate can be written as

$$E_p = E_0 e^{i\omega\left[t-(n-1)\frac{\Delta z}{c}-\frac{z}{c}\right]}, \tag{A.4}$$

that can be also be written as

$$E_p = e^{-i\omega(n-1)\frac{\Delta z}{c}} E_0 e^{i\omega\left(t-\frac{z}{c}\right)}, \tag{A.5}$$

which says that the wave after the plate is obtained from E_s by multiplying it by the factor $e^{-i\omega(n-1)\frac{\Delta z}{c}}$. When an oscillating function like $e^{i\omega t}$ is multiplied by a factor $e^{i\theta}$ it means that you are changing the phase of the oscillation by the angle θ. Indeed the extra delay in passing through the thickness Δz has retarded the phase by the amount $\omega(n-1)\Delta z/c$. Thus the effect of the plate is to multiply the field by a factor that shifts its phase. However instead of multiply E_s it is possible to obtain the same result by adding a suitable complex number. In the case that Δz is small it is possible to write

$$e - i\omega(n-1)\frac{\Delta z}{c} \approx 1 - i\omega(n-1)\frac{\Delta z}{c}, \tag{A.6}$$

by substituting it in Eq. 4.5 it is obtain

$$E_p = E_0 e^{i\omega\left(t-\frac{z}{c}\right)} - \frac{i\omega(n-1)\Delta z}{c} E_0 e^{i\omega\left(t-\frac{z}{c}\right)}. \tag{A.7}$$

Where the first term is the field from the source and the second term must be equal to the field produced to the right of the plate by the oscillating charges of the plate, depending on the strength of the wave from the source.
To calculate n it is now necessary to obtain the field produced from the oscillating charges, defined as E_a. If the source S is far off from the plate then the field E_s will have the same phase everywhere on the plate, so it is possible to write that in the neighbourhood of the plate the field is

$$E_s = E_0 e^{i\omega\left(t-\frac{z}{c}\right)}. \tag{A.8}$$

Each of the electrons in the atoms of the plate will be driven up and down by the electric force qE. To find the expected motion for the electrons these are assumed to behave like little oscillators with a resonant frequency ω_0. The equation of oscillators is:

$$F = m\left(\frac{d^2 x}{dt^2} + \omega_0^2 x\right), \tag{A.9}$$

where F is the driving force. Substituting the force $F = qE_s$ it is obtained

$$m\left(\frac{d^2 x}{dt^2} + \omega_0^2 x\right) = qE_0 e^{i\omega t}, \tag{A.10}$$

which solution is

$$x = \frac{qE_0}{m(\omega_0^2 - \omega^2)} e^{i\omega t}. \tag{A.11}$$

Remembering that the total field at a point P can be written as

$$E_p = -\frac{\eta q}{2\epsilon_0 c} \dot{x}_{t-\frac{z}{c}}, \tag{A.12}$$

where $\dot{x}_{t-z/c}$ is the velocity of charges at time $t - z/c$, and η is the number of atoms per unit area in the plate. Differentiating x in Eq. 4.11 and substituting it in Eq. 4.12 you obtain

$$E_a = -\frac{\eta q}{2\epsilon_0 c}\left[i\omega\frac{qE_0}{m(\omega_0^2 - \omega^2)} e^{i\omega\left(t-\frac{z}{c}\right)}\right]. \tag{A.13}$$

This expression is equal to the one obtained in Eq. 4.7 if

$$(n - 1)\Delta z = \frac{\eta q^2}{2\epsilon_0 m(\omega_0^2 - \omega^2)} , \tag{A.14}$$

substituting now Δz with η/N, where N is the number of atoms per unit volume of the plate, you get

$$n = 1 + \frac{Nq^2}{2\epsilon_0 m(\omega_0^2 - \omega^2)} . \tag{A.15}$$

Consider the formula just obtained. First of all, for most ordinary gases the natural frequencies of the electron oscillators correspond to ultraviolet light. These frequencies are higher than the frequencies of visible light, that is, ω_0 is much larger than ω of visible light, and to a first approximation it is possible to disregard ω^2 in comparison with ω_0^2. With this approximation the index is nearly constant. Thus for gases the index is nearly constant. Another important consideration is that as ω rises the index also rises. So n rises slowly with frequency, meaning that is higher for blue light than for red light. The phenomenon that the index depends upon the frequency is called the phenomenon of dispersion. Assume now to measure the index of refraction of a material like glass in the ultraviolet, where ω gets near ω_0. As the frequency gets very close to the natural frequency the index can get enormously large, because the denominator can go to zero. Next, suppose that ω is greater than ω_0. The term $\omega_0^2 - \omega^2$ becomes negative and n results to be less than one. That means that the effective speed of the waves in the substance is faster than c. This is correct, although it is said that you cannot send signals any faster than the speed of light. Indeed, it can be shown that the speed at which you can send a signal is not determined by the index at one frequency, but depends on what the index is at many frequencies. What the index tells is the speed at which the nodes of the wave travel.

The results obtained so far are somewhat simpler than you would actually find in nature. To be completely accurate some refinements have to be added. First, you should expect that the model of the atomic oscillator should have some damping force, otherwise once started it would oscillate forever. Adding a damping term the denominator becomes $\omega_0^2 - \omega^2 + i\gamma\omega$, where γ is the damping coefficient. You should take into account also the fact that there are several resonant frequencies for a particular kind of atom. It is easy to fix up the dispersion equation by imagining that there are several different kinds of oscillators and simply add the contributions of all the oscillators. Hence the obtained equation is

$$n = 1 + \frac{q^2}{2\epsilon_0 m} \sum_k \frac{N_k}{\omega_k^2 - \omega^2 + i\omega\gamma_k} . \tag{A.16}$$

In this last equation the index of refraction is a complex number that can be written as $n = n' - in''$. If you substitute this number in equation 4.5 you obtain

$$E_p = e^{-\omega n'' \frac{\Delta z}{c}} e^{-i\omega(n'-1)\frac{\Delta z}{c}} E_0 e^{i\omega\left(t - \frac{z}{c}\right)} , \tag{A.17}$$

where the last factors are just the form encountered before, and again describe a wave whose phase has been delayed by the angle $\omega(n'-1)\Delta z/c$ in traversing the material. The first term is an exponential factor with a real exponent that describes a decrease in the magnitude of the field. In fact as the wave goes through the material it is weakened by the material, that is absorbing part of the wave. Thus the imaginary part n" of a complex index of refraction represents absorption of the wave. Normally the absorption of light is very small. But if the light frequency ω is very close to ω_k then the resonance term $\omega_k^2 - \omega^2$ can become small compared with $i\omega\gamma_k$ and the index becomes almost completely imaginary, as shown in Fig. A.2. It is just this effect that gives the dark lines in the spectrum of light received from the sun. The light from the solar surface has passed through the sun's atmosphere and the light has been strongly absorbed in the resonant frequencies of the atoms in the solar atmosphere. The observation of such spectral lines in the sunlight allows you to determine the resonant frequencies of the atoms and hence the chemical composition of the sun's atmosphere.
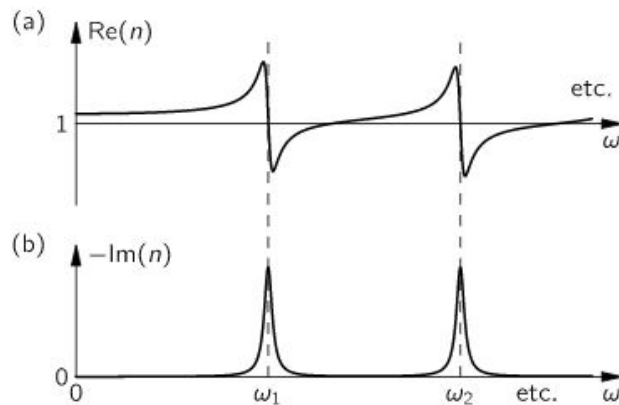
Fig. A.2. *The index of refraction as a function of frequency.*

All the results presented so far are valid only for low density materials, like gases. If you want to calculate the index of refraction of dense material you have to consider that charges' oscillations are driven not only by the incoming wave but also by the radiated waves of all the other atoms. If you're interested I suggest reading the chapters 10 and 31 of "The Feynman lectures on physics" Vol. II.

Sommario

La presente tesi tratta la progettazione del banco optomeccanico dell'invenzione HYPSOS (HYPerspectral Stereo Observing System). Questo innovativo strumento è stato concepito dal Prof. Naletto, dell'Università di Padova, dal Dott. Cremonese, dell'INAF, dalla Dott.sa Re, dell'Università di Parma, e dal Dott. Tordi, di EIE. Nell'arco dei sei mesi di lavoro di tesi, il candidato, sotto l'importante ed istruttiva guida del Prof. Naletto, ha progettato e disegnato le strutture meccaniche che sosterranno e permetteranno l'allineamento delle ottiche del banco ottico di HYPSOS.

1. Il lavoro di tesi

La tesi è suddivisa in quattro capitoli. Nei primi tre capitoli vengono introdotti alcuni principi fondamentali di ottica, le configurazioni dei due strumenti che hanno ispirato HYPSOS, e la configurazione di HYPSOS stesso. Nel quarto capitolo, invece, viene presentato il lavoro svolto nella progettazione del banco optomeccanico di HYPSOS.

1.1. Capitolo 1

Prendendo ispirazione dai libri *"Optics"* di Hecht, e *"The Feynman Lectures on Physics"* di Feynman, nel primo capitolo sono descritti alcuni concetti fondamentali di ottica. Partendo dalla definizione di radiazione si descrive la natura della luce e le principali leggi fisiche che la governano. Tuttavia la luce visibile è solo una piccola parte del più vasto spettro radiativo, per questo vengono presentate le differenti bande spettrali, partendo da quelle con energia minore, o lunghezza d'onda maggiore. Viene quindi presa in considerazione l'ipotesi di ottica geometrica, un'approssimazione valida quando la luce interagisce con oggetti le cui dimensioni sono molto maggiori della sua lunghezza d'onda. Mediante questa ipotesi, per cui è possibile descrivere il fascio luminoso come un raggio rettilineo, si derivano le equazioni caratteristiche delle lenti e degli specchi.

Si passa quindi alla descrizione del funzionamento di un generico telescopio: questo strumento permette di vedere un oggetto distante aumentandone la sua dimensione apparente sulla retina del nostro occhio. Nell'ambito di questo lavoro di tesi si descrivono brevemente le configurazioni (Fig. 1.) del telescopio di Schmidt e quella del telescopio TMA (three-mirror anastigmat). La prima utilizza uno specchio primario sferico e una lente correttrice asferica posta nel centro di curvatura dello specchio primario, mentre il rivelatore è posto nel fuoco dello specchio primario. Un telescopio TMA, invece, è composto da tre specchi curvi che permettono di minimizzare tutte e tre le principali aberrazioni.
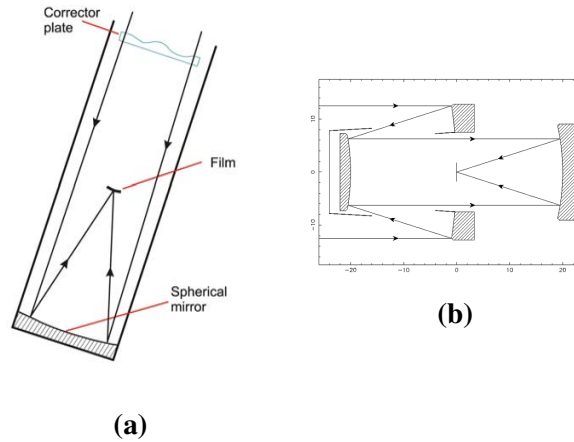
Fig. 1. *Configurazione di Schmidt (a) e TMA (b)*

Non considerando più l'ipotesi di ottica geometrica si deve tener conto delle diverse aberrazioni provocate dai raggi fuori dal piano o distanti dal centro della lente. Vengono quindi analizzate le principali aberrazioni che possono influenzare un generico strumento ottico. Nonostante i moderni telescopi siano in grado di eliminare gli errori provocati dalle aberrazioni vi è comunque un limite fisico per la risoluzione di un qualsiasi strumento. Questo è legato al fenomeno della diffrazione della luce ed uno strumento che lavora al suo limite teorico è detto "limitato dalla diffrazione".
Inoltre in questo capitolo è descritto anche un altro fenomeno fondamentale nello studio della luce: l'interferenza. Infatti, studiando la sovrapposizione di due o più onde si può osservare come l'intensità dell'onda risultante possa variare tra un minimo, in corrispondenza del quale non si osserva alcun fenomeno ondulatorio, ed un massimo, uguale alla somma delle intensità delle singole onde. Questo fenomeno è alla base del funzionamento degli spettrometri. In questi strumenti un reticolo di diffrazione provvede a scomporre il fascio nelle diverse lunghezze d'onda, che poi vengono assorbite e codificate da un rivelatore. Di particolare interesse per la comprensione di HYPSOS è la tecnica dell'iperspettroscopia. Grazie a questa si ottiene un cubo iperspettrale composto da due dimensioni spaziali e da una dimensione spettrale. Un insieme di dati fondamentale per le future esplorazioni planetarie.
Nella parte conclusiva del capitolo si descrive brevemente il processo di ricostruzione DTM (digital terrain model) a partire dalle immagini stereoscopiche acquisite. Il modello utilizzato è il software DM sviluppato dall'Università di Parma.

1.2. Capitolo 2

Nella parte introduttiva del secondo capitolo viene brevemente trattata la missione Bepi Colombo. Questa missione, lanciata il 20 ottobre 2018, ha come obiettivo lo studio della superficie e della magnetosfera di Mercurio. Si pensa che i dati acquisiti permetteranno di ottenere importanti informazioni riguardanti l'origine del nostro Sistema Solare e del pianeta stesso. Tra gli strumenti a bordo della missione risultano di particolare importanza, nell'ambito di questa tesi, la stereocamera STC (Stereoscopic Imaging Channel) e l'iperspettrometro VIHI (Visible and Infrared Hyperspectral Imager). Questi due strumenti hanno infatti ispirato il concetto di HYPSOS. Il primo, STC, è una camera con due canali stereoscopici progettata per acquisire immagini della superficie di Mercurio con due diverse angolazioni. Il suo design ottico consiste in un telescopio di Schmidt modificato e in due prismi romboidali. La sua peculiarità è il detector in comune per i due diversi canali. Le immagini ottenute, usando la tecnica push-frame, verranno utilizzate per ricostruire il DTM della superficie del pianeta. Il secondo, VIHI, è un iperspettrometro che permetterà di riprodurre una mappa mineralogica della superficie di Mercurio. Il suo design ottico consiste in un telescopio di Schmidt modificato e da uno spettrometro Littrow. Lo strumento acquisirà i dati utilizzando la tecnica push-broom, ovvero combinando frames sequenziali acquisiti sfruttando il moto del satellite.

Nella parte conclusiva del secondo capitolo viene descritto SVS (Stereo Validation Setup), il banco da lavoro utilizzato per la caratterizzazione di STC. In questo setup di laboratorio un target, che simula la superficie da osservare, viene illuminato da una fonte luminosa mobile, con la possibilità di ottenere diversi angoli di incidenza. La luce riflessa dall'oggetto viene concentrata da un collimatore che la invia verso lo strumento. Sia il prototipo sia il target sono montati su dei rotori che permettono di simulare il movimento relativo tra lo strumento e l'obiettivo. Una volta generato il DTM, questo viene confrontato con i dati ricavati utilizzando uno scanner laser.
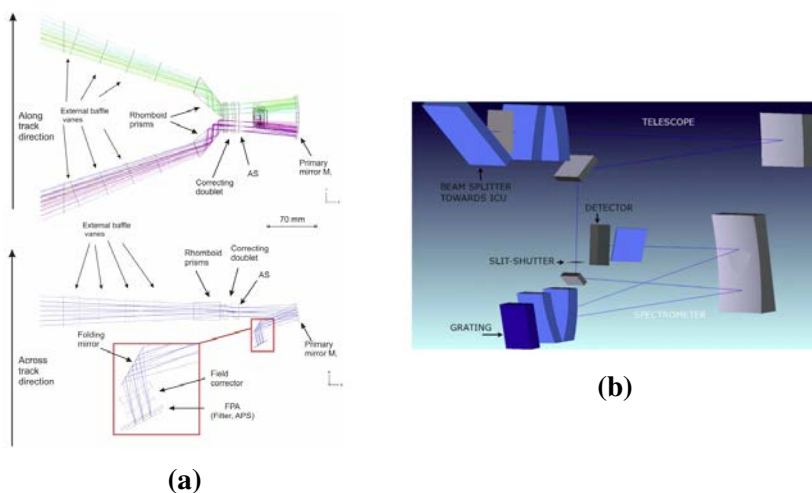

(a)

(b)

Fig. 2. *Il design ottico di VIHI (a) e STC (b)*

1.3. Capitolo 3

Il terzo capitolo si occupa del design ottico e della caratterizzazione di HYPSOS. In questi ultimi anni si sta assistendo ad un'evoluzione delle missioni di esplorazione planetaria: dopo una fase iniziale in cui i principali pianeti del nostro Sistema Solare sono stati sorvolati per la prima volta, le agenzie spaziali stanno focalizzando i loro sforzi sulla ricerca di possibili tracce di composti organici. Con l'evoluzione degli obiettivi di missione sono quindi necessari nuovi strumenti di bordo. In particolare, in questi innovativi studi, la ricostruzione tridimensionale della superficie planetaria e le informazioni spettrali ad essa associate diventano di fondamentale importanza. Se difatti si analizzano le missioni di esplorazione planetaria del recente passato e del prossimo futuro tutte hanno a bordo una telecamera stereoscopica ed una telecamera multispettrale. Si pensi, ad esempio, alla missione BepiColombo, in viaggio verso Mercurio, ed alla missione Juice, prevista in partenza per il 2022 con obiettivo Giove. Tuttavia la sintesi dei dati forniti da questi due strumenti comporta un peggioramento della qualità dei risultati finali, a causa delle differenti risoluzioni spaziali e spettrali, ed una maggiore incertezza, dovuta alle differenti procedure di calibrazione degli strumenti. Inoltre l'acquisizione delle immagini superficiali è inficiata da possibili errori causati dalle variazioni delle condizioni atmosferiche locali, dai diversi angoli di incidenza della luce solare e dalle differenti temperature superficiali. Il concetto di HYPSOS è nato con l'intento di mitigare queste problematiche. Questo innovativo strumento, attualmente in sviluppo presso l'Università di Padova, è un dispositivo stereo-iperspettrale che unisce le funzioni di una telecamera stereoscopica e di un iperspettrometro. Essendo uno strumento unico verrebbero eliminati i problemi legati all'elaborazione dei dati provenienti da diversi strumenti, causati dalle loro diverse caratteristiche metrologiche. Inoltre HYPSOS permetterà di calibrare e validare i dati iperspettrali direttamente dalle immagini acquisite. Difatti, dalla misura dello spettro del punto topografico più alto e di quello più basso, sarà possibile calcolare il contributo dell'atmosfera locale, migliorando l'identificazione delle specie minerali ivi presenti. Infine l'utilizzo delle immagini a colori per la ricostruzione dei digital terrain model permetterà di ottenere dei modelli della superficie più accurati e con una risoluzione maggiore. Le immagini a colori infatti contengono più informazioni rispetto alle immagini in bianco e nero solitamente utilizzate per la generazione dei DTM. Inoltre, come dimostrato in vari studi scientifici (Bleyer & Chambon (2010) e Galar (2013)), l'utilizzo di immagini a colori comporta una riduzione degli errori di correlazione fino al 25%. Oltre a presentare questi vantaggi, sta venendo anche studiata la possibilità di utilizzare questo innovativo strumento in future missioni nell'ambito dell'osservazione terrestre, a bordo di un cubesat.

Il capitolo prosegue studiando il design ottico di HYPSOS. Questo è ispirato a quello della stereo camera STC a bordo della missione BepiColombo. Le immagini, come per STC, vengono acquisite da due aperture, poste rispettivamente a ±20° rispetto al nadir del satellite. Tuttavia, diversamente da STC, le immagini vengono generate sfruttando la tecnica push-broom, ovvero combinando frames sequenziali acquisiti sfruttando il moto del satellite. Un'altra differenza rispetto al layout ottico di STC è l'introduzione di una fenditura e di uno spettrometro. Per poter utilizzare un solo spettrometro è necessario che i due canali stereo nel piano focale del telescopio siano orientati in modo che le due immagini abbiano la stessa direzione. Per questo scopo vengono utilizzati due prismi di Pechan, uno per ogni canale stereo, opportunamente orientati. Una volta orientati, i due fasci luminosi passano attraverso due distinte zone della fenditura, posta nel piano immagine comune. I due fasci vengono quindi dispersi da un reticolo di diffrazione ed inviati, scomposti nelle differenti lunghezze d'onda, al sensore bidimensionale. Con i dati così ottenuti HYPSOS permetterà di riprodurre un hyperspectral digital terrain model (HDTM), associando ad ogni porzione del modello tridimensionale del terreno il suo spettro.

In questo design ottico la scelta dello spettrometro risulta di fondamentale importanza. Sono state valutate due possibili soluzioni: uno spettrometro di tipo Offner, e uno di tipo Wynne-Dyson. Il primo ha il vantaggio di non presentare aberrazioni cromatiche, essendo completamente composto da specchi. Il suo principale svantaggio è legato alle dimensioni maggiori e all'elevato costo di produzione del reticolo convesso. Il secondo, invece, è un design più appropriato per estendere il range spettrale alle lunghezze d'onda dell'infrarosso. Il suo principale svantaggio è la vicinanza della fenditura al rivelatore.

Attualmente lo strumento sta venendo sviluppato da un team multidisciplinare sotto la supervisione del Prof. Naletto Giampiero, dell'Università di Padova, e del Dott. Cremonese Gabriele, dell'INAF. La costruzione del prototipo è finanziata dell'ASI con un contratto iniziato a febbraio 2020 per un periodo totale di due anni. Questo contratto prevede la realizzazione dello strumento e la sua caratterizzazione ed analisi prestazionale. Una volta assemblati il telescopio e lo spettrometro, questi dovranno essere integrati nel layout ottico. Durante questa fase verrà posta particolare attenzione alla modularità dello strumento, sarà infatti necessario caratterizzare prima il solo telescopio, e quindi inserire successivamente lo spettrometro. Questo per ricavare le prestazioni di ricostruzione dell'immagine prima della sua dispersione, informazioni che saranno fondamentali nella ricostruzione stereoscopica. In questa fase verrà svolta anche la calibrazione geometrica dei due canali, misurandone la lunghezza focale, la funzione di diffusione del punto (PSF) e la distorsione geometrica. Lo spettrometro verrà invece caratterizzato usando una fonte luminosa monocromatica variabile. Una volta caratterizzati, i due sottosistemi dovranno essere allineati cercando di ottenere la perfetta sovrapposizione tra la fessura e il piano focale del telescopio stesso. Questo compito sarà estremamente delicato ed è reso ancora più complesso dalle limitate dimensioni fisiche della struttura.

La caratterizzazione di HYPSOS può essere suddivisa in due principali compiti: da una parte la calibrazione ottica, descritta in precedenza, dall'altra la calibrazione della ricostruzione stereoscopica, in cui viene valutata la precisione della ricostruzione 3D dello strumento. Mentre la prima è una procedura standard, la seconda sarà la prima volta in assoluto che viene svolta in laboratorio. Per la caratterizzazione stereo verrà utilizzato SVS (Stereo Validation Setup), il sistema già usato per la caratterizzazione della STC di Bepicolombo. Tuttavia, rispetto al sistema utilizzato per STC, saranno applicate due modifiche. Acquisendo HYPSOS in push broom, sarà necessario avere una rotazione continua e coordinata del prototipo e dell'obiettivo. L'altra modifica riguarderà il sistema di illuminazione del target: al posto di una lampada alogena verrà utilizzata una lampada capace di fornire diversi range spettrali di illuminazione. I parametri intrinseci dello strumento, la cui conoscenza è fondamentale per l'accuratezza della ricostruzione 3D, verranno calcolati utilizzando l'algoritmo di Zhang. Essendo la prima volta che tale tecnica viene usata per caratterizzare uno strumento che lavora in modalità push broom, inizialmente verrà utilizzato solamente il telescopio. Questo permetterà di verificare la capacità di ricostruzione dell'immagine bidimensionale del prototipo. Una volta confermata, si eseguirà la caratterizzazione spettrale dell'immagine aggiungendo anche lo spettrometro. Dall'analisi delle coppie di immagini, ottenute illuminando la scacchiera di Zhang con una lampada spettrale, si otterranno i parametri intrinseci, per ogni coppia di immagini, dipendenti dalla lunghezza d'onda della fonte luminosa. Una volta ottenute queste informazioni sarà finalmente possibile ottenere un ipercubo per ogni canale stereo. Un ipercubo consiste in un cubo di tre dimensioni (x,y,λ), dove x ed y rappresentano le dimensioni spaziali e λ la dimensione spettrale. Gli ipercubi così ottenuti verranno utilizzati per testare l'accuratezza dell'algoritmo di ricostruzione 3D della superficie, confrontando la DTM prodotta dall'algoritmo con quella generata utilizzando uno scanner laser.
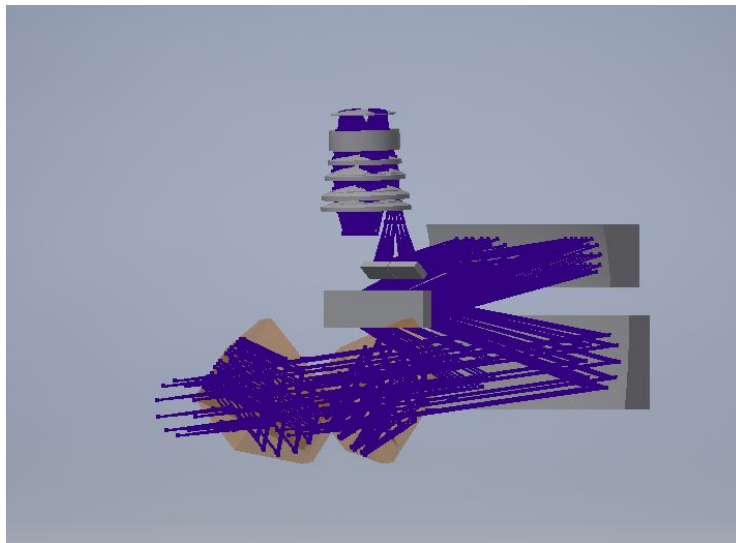

Fig. 3. *Il design ottico di HYPSOS*

1.4. Capitolo 4

Nel quarto capitolo è descritta la progettazione delle varie componenti che comporranno il banco optomeccanico del prototipo di HYPSOS.

Uno dei grandi vantaggi di HYPSOS è la possibilità di unire due tipologie di strumenti in un singolo oggetto. Questo, oltre a comportare vantaggi nella calibrazione, potrebbe implicare un minore volume occupato, un vantaggio fondamentale in previsione di future missioni di osservazione della Terra tramite cubesat. Per questo si è cercato di mantenere la struttura la più piccola possibile. Questo però comporta un minor spazio disponibile e la necessità di un accurata progettazione per rispettare i requisiti richiesti da ogni componente durante il processo di allineamento.
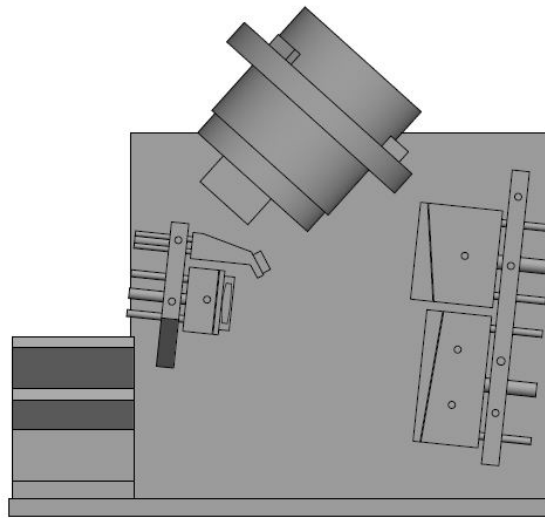
Fig. 4. *Il banco ottico di HYPSOS*

Per semplificare la progettazione, si è deciso di suddividere l'inteara struttura in sei diverse sotto-sezioni:

- il telescopio TMA, composto da due specchi concavi ed uno convesso;

- lo specchio piano;

- lo spettrometro, composto da cinque diverse lenti e da un reticolo;

- l'insieme fenditura-rivelatore, composto da una struttura che sosterrà la fenditura e il rivelatore;

- i rotatori di campo, composti da due prismi di Pechan;

- la struttura, che consiste nelle pareti e negli otturatori interni.

1.4.1 Il telescopio

Il telescopio TMA consiste in tre specchi sferici. M1 e M3 sono specchi concavi, mentre M2 è uno specchio convesso. Prima della caratterizzazione di tutto il prototipo, il telescopio dovrà venire allineato. Per fare questo è necessario che i tre specchi possano muoversi indipendentemente lungo gli assi xyz e possano ruotare lungo gli assi di tip e tilt, per un totale di cinque gradi di libertà (Fig. 5.).
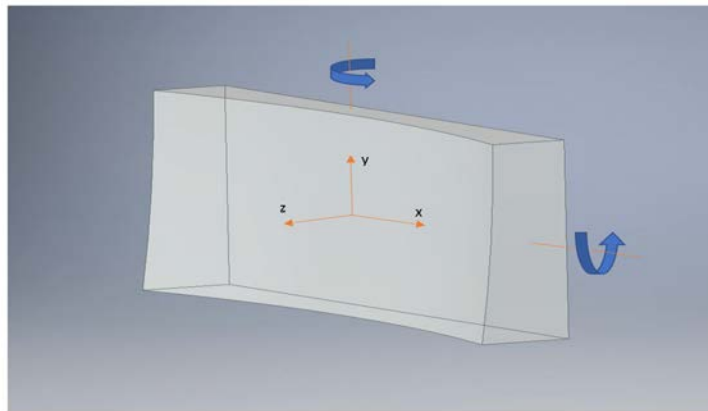

Fig. 5. *I gradi di libertà richiesti da ogni specchio.*

Per rispettare questi requisiti sono stati progettati tre diversi supporti in alluminio. I meccanismi che garantiranno l'allineamento sono uguali per tutti e tre gli specchi. Il movimento lungo gli assi x e y è garantito dal movimento di alcuni grani posizionati lungo i lati dei supporti. Per questo il foro centrale di ogni supporto è stato progettato con un gioco di 1.5 mm. Tuttavia, a causa dell'impossibilità di accedere ad alcuni grani per la vicinanza con altri oggetti, i lati superiori di M1 ed M2, ed il lato inferiore di M3 non saranno dotati di grani, ma verranno utilizzate delle molle elicoidali. Per evitare di danneggiare gli specchi, i grani saranno in plastica e con la testa piatta. Sul retro di ogni supporto sono stati previsti quattro fori. Il foro centrale verrà usato per inserire una vite (di diametro M8 per M1 ed M3, di diametro M6 per M2) che permetterà la traslazione lungo l'asse z e sosterrà il supporto. Questa vite centrale sarà filettata alla parete e verrà regolata da un dado esterno. Negli altri tre fori, posti in una configurazione ad L, verranno inserite tre viti M4 che permetteranno le rotazioni di tip e tilt. Queste viti verranno fissate direttamente al supporto, anche usando della colla per assicurarne il fissaggio; i fori della parete saranno invece leggermente più larghi per permettere un minimo movimento per le viti. Data la grande precisione richiesta, la tolleranza richiesta per la filettatura dei tre fori sul retro del supporto è 4H.
Per garantire la stabilità degli specchi all'interno dei supporti questi verranno fissati con una cornice di materiale plastico. Questa spingerà lo specchio verso due molle elicoidale, poste alla base del supporto.

Nonostante il meccanismo di allineamento sia comune a tutti gli specchi, a causa delle diverse forme e dei diversi pesi i supporti risultano molto diversi tra loro. M1 e M3, essendo più grandi di M2, necessitano di un supporto più spesso, capace di reggerne il peso. Per questo il loro supporti hanno uno spessore di 8 mm su ogni lato, a parte per i due lati più vicini, che sono spessi solo 5 mm per motivi di spazio. Per quanto riguarda invece il supporto di M2, questo è spesso solamente 5 mm. Ad eccezione dei due lati laterali che sono più spessi per motivi di spazio legati alla cornice. Anche le cornici risultano molto diverse tra di loro. Quelle per M1 e M2 seguono la forma del supporto per ottenere, una volta fissate, un parallelepipedo rettangolo. La cornice di M2, invece, segue la curvatura dello specchio. Inoltre, per evitare di graffiare la superficie dello specchio, verrà poggiata su esso solamente con un riquadro di 1 mm di larghezza. I fori sulla cornice sono stati previsti più larghi per consentire il movimento solidale della cornice con lo specchio durante l'allineamento. Tutte le cornici hanno un foro centrale che verrà utilizzato per allineare il telescopio tramite un fascio laser. Questi fori, una volta allineato il telescopio, saranno chiusi con degli appositi dadi, per quanto riguarda M1 ed M3, e con un tappo di plastica, per M2.

I supporti verranno realizzati dall'officina meccanica dell'osservatorio di Asiago, mentre le cornici verranno stampate presso il CISAS.

Per verificare che le cornici non provochino un'eccessiva deformazione sugli specchi, è stata condotta un'analisi degli stress su ogni specchio del telescopio. Per prima cosa si è riprodotto il file 3D dello specchio, per poi calcolare, per mezzo di un'analisi agli elementi finiti, le deformazioni provocate dalle cornici. Il tutto è stato fatto utilizzando il software Inventor.

La massima deformazione tollerata è definita da $\lambda/20$, dove $\lambda = 630$ nm è la lunghezza d'onda di riferimento per un laser HeNe. Nella tabella seguente sono riportate le forze di compressione massime tollerate.

Specchio	Massima compressione (N)	Massima deformazione (nm)
M1	6	30
M2	3	23
M3	4	32

1.4.2 Lo specchio piano

Lo specchio piano ha il compito di riflettere il piano focale del telescopio nella posizione desiderata. Quindi il suo posizionamento definisce anche quello dello spettrometro e del supporto per la fenditura e il rivelatore. L'angolo dello specchio piano e la sua distanza da M3 sono stati scelti tenendo in considerazione i seguenti vincoli (Fig. 5.):

a) la distanza tra il supporto dello specchio piano e il fascio tra M2 ed M3 non deve essere minore di 4 mm;

b) la distanza tra il supporto dello specchio piano e il supporto di M2 deve essere almeno di 5 mm;

c) l'angolo dello specchio piano deve essere tale che la distanza tra il supporto dello specchio piano e il rivelatore sia di almeno 10 mm;

d) l'angolo dello specchio paino deve essere tale che la distanza tra il supporto dello spettrometro e il fasci tra M3 e lo specchio piano sia di almeno 10 mm.

Per rispettare questi vincoli è stato scelto un angolo di 34° rispetto il la superficie posteriore di M3 ed una distanza di 127 mm da M3.
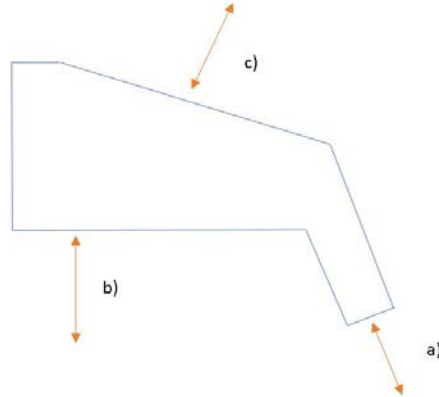

Fig. 5. *I vincoli richiesti nella scelta della posizione dello specchio piano.*

Durante l'assemblaggio dello strumento la possibilità di muovere lo specchio piano sarà fondamentale per garantire un più facile allineamento tra il telescopio e lo spettrometro. Come per gli specchi del telescopio si utilizzano quattro viti per permettere i movimenti necessari. Le tre viti più piccole, disposte a L, garantiscono le rotazioni di tip-tilt. La vite centrale, invece, garantisce la traslazione lungo l'asse z e regge il supporto. Come per i supporti degli specchi del telescopio, data la grande precisione richiesta, la tolleranza dei fori è di 4H. Lo specchio verrà incollato al supporto senza aver la possibilità di essere mosso lungo gli assi x e y.

1.4.3 Lo spettrometro

Lo spettrometro è composto da cinque lenti concentriche di dimensioni diverse, e da un reticolo. Tutti questi componenti verranno inseriti in un cilindro, che sarà sviluppato dallo stesso produttore delle lenti e dello specchio piano. L'allineamento dello spettroemtro con il telescopio è di fondamentale importanza per il corretto funzionamento del prototipo. Per questo lo spettrometro dovrà poter essere mosso con i gradi di libertà richiesti (Fig. 6.)
Il cilindro verrà fissato ad un anello di supporto tramite sei viti, tre saranno filettate all'anello di supporto, mentre le altre tre saranno filettate al cilindro. Questo garantirà, come per i supporti del telescopio, di ottenere i gradi di libertà richiesti. L'anello esterno sarà fissato a sua volta alle due pareti laterali tramite due strutture simmetriche.

Queste sono state progettate per fornire la necessaria rigidità richiesta dal supporto. Si pensi, infatti, che qualunque minimo movimento della fenditura comporta un'importante modifica delle informazioni ricevute dal rivelatore. Le strutture di sostegno hanno due fori rettangolari sulla parte superiore e tre viti di fissaggio, per permettere la traslazione lungo gli assi x e y. La traslazione lungo z è possibile utilizzando degli opportuni spessori. Per lasciare una certa libertà di movimento all'anello, i fori dell'anello sono più larghi di quelli dei supporti. Data la complessa forma dei supporti di sostegno questi saranno stampati presso i laboratori del CISAS, mentre l'anello esterno sarà fabbricato insieme agli altri supporti.
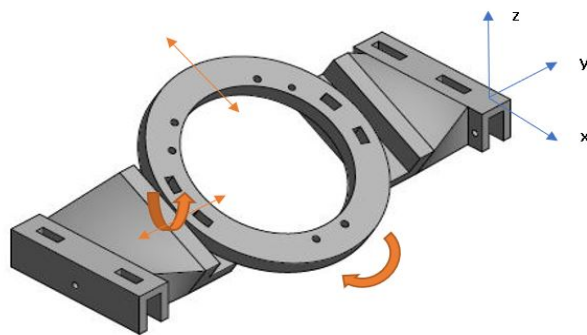

Fig. 6. *I gradi di libertà richiesti dallo spettrometro.*

1.4.4 Il supporto della fenditura e del rivelatore

L'allineamento della fenditura e del rivelatore è di fondamentale importanza. Per questo motivo di è deciso di inserire i due oggetti in una singola struttura di supporto che verrà fissata al cilindro dello spettrometro. L'ulteriore vantaggio di questo supporto è che ridurrà la luce diffusa entrante all'interno dello spettrometro. Il supporto consiste in una struttura cilindrica con all'interno due fori. Uno permetterà al fascio proveniente dallo specchio piano di raggiungere lo spettrometro, passando per la fenditura. Mentre l'altro sarà utilizzato per fissare il rivelatore. La fenditura, essendo molto sottile e fragile, verrà inserita in un supporto rettangolare, e mantenuta fissa tramite una cornice. Entrambi gli oggetti avranno la possibilità di essere allineati utilizzando degli opportuni spessori.
Durante la caratterizzazione dello strumento in laboratorio verrà utilizzato un rivelatore board level, è quindi necessario evitare cariche elettrostatiche che potrebbero danneggiare irrimediabilmente il rivelatore. Per questo anche questo supporto verrà stampato in un materiale plastico non conduttore presso i laboratori del CISAS.

1.4.5 I rotatori di campo

I rotatori di campo consistono in due prismi di Pechan. Questi sono usati per ruotare il fascio luminoso entrante di 90° per avere le due immagini sullo stesso piano. Per ottenere questa rotazione i due prismi devono essere ruotati di 45° rispetto alla base del banco ottico. Ogni piccola deviazione da questa angolo causa un disallineamento delle due immagini, è quindi di fondamentale importanza che i due prismi siano fissati rigidamente e correttamente inclinati. Per fissare i prismi di Pechan con l'angolo corretto è stato progettato un supporto composto di due diversi pezzi. La base sarà fissata al banco ottico con quattro viti M5, assicurandone la corretta inclinazione di 45°; mentre la struttura ad U permetterà di fissare il prisma in posizione con quattro viti M3. Le due parti del supporto saranno fissate tra loro per mezzo di quattro viti M5.

1.4.6 Le pareti

Le pareti devono essere spesse a sufficienza da sostenere il peso complessivo del banco ottico. La base avrà uno spessore di 15 mm, mentre le altre pareti saranno spesse 10 mm. Nel design ottico il telescopio è inclinato di 6° rispetto al fascio luminoso entrante. Per semplificare la progettazione dei fori si è scelto di inclinare le pareti di sostegno degli specchi del telescopio dello stesso angolo. Queste pareti saranno fissate e sostenute dalle pareti laterali. Le pareti laterali, invece, saranno fissate alla base del banco ottico. Per poter garantire l'accesso ai grani durante l'allineamento sono stati predisposti tre fori su ciascuna delle due pareti laterali. Inoltre per diminuire la luce diffusa all'interno dello strumento sono stati predisposti anche degli otturatori interni.

2. Conclusioni

In questa tesi è stato presentato il lavoro svolto dal candidato negli ultimi sei mesi nella progettazione del banco ottico di HYPSOS. Tuttavia la configurazione ottica di alcuni componenti devono ancora venire congelata. Per questo alcuni disegni tecnici, descritti in questa tesi, potrebbero essere non quelli definitivi.
Si prevede di terminare un primo modello, stampando tutte le principali componenti presso il CISAS, per la fine di novembre; mentre il banco vero e proprio dovrà essere assemblato per la fine di gennaio, data di arrivo degli specchi del telescopio.
La progettazione di componenti innovativi ed originali si è rilevato essere un lavoro molto stimolante, in cui il candidato ha avuto la fortuna di essere consigliato da persone altamente qualificate. In definitiva il banco progettato può essere racchiuso in un solido con dimensioni 230x310x250 mm^3, potendo allineare qualunque componente mantenendo chiuso il banco.